Characterization of the inhibitory potential of novel inhibitors of human Dimethylarginine Dimethylaminohydrolase 1 (*h*DDAH1)

Figure removed due to copyright restriction

Crystallographic structure of human DDAH1.
Source: https://en.wikipedia.org/wiki/Dimethylargininase.

Master of Biotechnology

by

VANESSA LEMES DO NASCIMENTO

Supervisors: Dr. Sara Tommasi and Prof. Arduino A. Mangoni.

Department of Clinical Pharmacology

College of Medicine and Public Health

Flinders University

Jan 2022

Master of Biotechnology

College of Medicine and Public Health

Flinders University

TOPIC

BTEC9000A Biotechnology Research Project (Medicine) 2021 S1

TITLE OF THE STUDY

Characterization of the inhibitory potential of novel inhibitors of human Dimethylarginine Dimethylaminohydrolase 1 (*h*DDAH1).

STUDENT NAME

VANESSA LEMES DO NASCIMENTO

STUDENT ID

2243897

SUPERVISOR NAME AND ADDRESS

Dr. Sara Tommasi Department of Clinical Pharmacology - FMC (6D215)

CO-SUPERVISRO NAME AND ADDRESS

Professor Arduino A. Mangoni Department of Clinical Pharmacology - FMC

EXAMINER 1 NAME AND ADDRESS

A. Professor Robyn Meech Department of Clinical Pharmacology - FMC (6D322)

EXAMINER 2 NAME AND ADDRESS

Dr Janet Coller School of Biomedicine, University of Adelaide, L2, Helen Mayo South

ABSTRACT

Nitric Oxide (NO) is a gaseous signalling molecule that is produced by virtually all organisms, from bacteria to plants and animal cells. NO plays a crucial role in many biological processes. However, an excessive production of this molecule can be detrimental, contributing to the development of many pathological conditions. NO is synthesised from L-arginine via a reaction catalysed by the enzyme nitric oxide synthase (NOS). The activity of NOS is inhibited by the methylated arginines asymmetric dimethylarginine (ADMA) and monomethyl arginine (L-NMMA), that act as endogenous competitive inhibitors of all three isoforms of NOS (nNOS, eNOS, iNOS). Both ADMA and L-NMMA are metabolised by the cytosolic enzyme dimethylarginine dimethylaminohydrolase 1 (*h*DDAH1) into L-citrulline (CIT) and dimethylamine (DMA) or monomethylamine (MMA), respectively. Two isoforms of DDAH have been reported in humans, identified as DDAH1 and dimethylarginine dimethylaminohydrolase 2 (DDAH2), but DDAH1 appears to be the major player in methylated arginine metabolism. Thus, *h*DDAH1 is a crucial NO modulator and inhibition of *h*DDAH1 activity results in the accumulation of ADMA and L-NMMA and the consequent inhibition of NOS. Furthermore, enhanced *h*DDAH1 expression has been linked to several pathophysiological conditions and there is increasing evidence demonstrating its role as an emerging therapeutic target to excessive NO production.

In this research project, the potential of seven novel compounds to act as *h*DDAH1 inhibitors was measured; six of these molecules identified through Artificial Intelligence (AI) and one compound specifically designed within our lab using the known *h*DDAH1 inhibitor ZST316 as a template. A robust Ultra-Performance Liquid Chromatography – coupled to Mass Spectrometry (UPLC-MS) based *h*DDAH1 activity assay was also developed and used to measure *h*DDAH1 catalysed CIT formation. Method validation included the determination of instrument and method precision, intra- and inter-day variability and accuracy, robustness,

linearity, and lower limit of detection (LLOD) and quantification (LLOQ). The assay was also investigated for protein and time linearity and the model that best describe the enzyme kinetics identified, followed by screening of the inhibitory potential of seven novel compounds. This research proposal hypothesised that at least one of the seven screened compounds would act as a *h*DDAH1 inhibitor with a constant of inhibition (K_i) <10 μM and/or half maximal inhibitory concentration (IC_{50}) <20 μM. The method developed was robust, reproducible, precise (%CV < 11%), and accurate (accuracy between 101 and 105 %). LLOD was 0.4 μM, LLOQ was 1 μM and calibration curves were always linear. A linear relationship was observed between the concentration of CIT formed and total protein concentration and incubation time and the Michaelis Menten model best fit the enzymatic system, with K_m of 112 ± 9 μM and V_{max} of 839 ± 23 pmol*min^{-1}*mg^{-1}. According to the findings, none of the screened compounds designed by AI acted as a *h*DDAH1 inhibitor, however the compound designed within the Clinical Pharmacology lab, ZIR26, has exhibited an estimated IC_{50} comprised between 1 and 10 μM. This supports the hypothesis and should be explored further in future experiments. Future perspectives include the screening of the remaining 64 potential inhibitor identified by AI, full kinetic characterisation of novel inhibitors and investigation of *h*DDAH1 inhibition in cellular and animal models of diseases characterised by excessive NO synthesis.

DECLARATION

‘I certify that this thesis does not contain material which has been accepted for the award of any degree or diploma; and to the best of my knowledge and belief it does not contain any material previously published or written by another person except where due reference is made in the text of this thesis.’

Vanessa Lemes do Nascimento

24 January 2022

ACKNOWLEDGEMENTS

First and foremost, I would like to express my deep and sincere gratitude to my research supervisor, Dr. Sara Tommasi, for giving me the opportunity to do research and providing invaluable guidance throughout my research work to complete this successfully.

I would also like to thank my co-supervisor, Prof Arduino Aleksander Mangoni. His dynamism, sincerity and motivation have deeply inspired me. Thank you for your empathy, and great sense of humour. Also, a huge thanks to my research colleagues from Clinical Pharmacology Department, Dr Pramod Nair and Anthony Doman for helping me and to contribute to this work.

I am extremely grateful to my friends for their love, caring and for believing in me. I am very much thankful to my family for their love, prayers, and continuing support to complete this research work.

Last but not least, thank you to my husband, André Freitas: my deepest gratitude. Your encouragement when the times got rough are much appreciated. It was a great comfort and relief to know that you were willing to provide management of our household activities while I completed my work. My heartfelt thanks.

Finally, thanks go to all the people who have supported me to complete the research work directly or indirectly and to all my master students colleagues.

TABLE OF CONTENTS

LIST OF FIGURES

LIST OF TABLES

ABBREVIATIONS AND SYMBOLS

A01- F01	Inhibitor Candidate by Atomwise
ADMA	Asymmetric Dimethylarginine
AGAT	Arginine:Glycine Amidinotransferase
AGTX2	Alanine Glyoxylate Aminotransferase 2
AI	Artificial Intelligence
Asp126	Aspartic Acid Aminoacid
BSA	Bovine Serum Albumin
Cl-NIO	N5-(1-Imino-2-Chloroethyl)-L-Ornithine Dihydrochloride
CIT	Citrulline
CIT-d6	L-Citrulline-D6
C_{max}	Maximum Serum Concentration
CO2	Carbon Dioxide
CV	Coefficient Of Variation
Cys273	Cyteine Aminoacid
DDAH1 and 2 ***h*DDAH1**	Dimethylarginine Dimethylaminohydrolase-1 And 2
DD1E5	Small Molecule Inhibitors
DD1C7	Small Molecule Inhibitors
DD1G7	Small Molecule Inhibitors
DMA	Dimethylamine
DMEM	Dulbecco's Modified Eagle's Medium
DMSO	Dimethyl Sulfoxide
DNA	Deoxyribonucleic Acid

eNOS	Endothelial Nitric Oxide Synthase
F%	Oral Bioavailability
FBS	Foetal Bovine Serum
FVB	Albino, Inbred Laboratory Mouse
HEK293T	Human Embryonic Kidney (293t)
His172	Histidine Aminoacid
IC_{50}	Half Maximal Inhibitory Concentration
iNOS	Inducible Or Inflammatory Nitric Oxide Synthase
IS	Internal Standard
kDa	Kilodalton
Kg	Kilogram
K_i	Constant Of Inhibition
K_m	Saturation By the Substrate
L-257	Small Molecule Inhibitors
L-CIT	L-Citrulline
LLOD	Lower Limit of Detection
LLOQ	Lower Limit of Quantification
L-NMMA	Ng-Monomethyl-L-Arginine Acetate
LPS	Lipopolysaccharides
M	Molar
mg	Milligram
miRNA	Micro rna
MEM	Non-Essential Amino Acids
mL	Millilitre
mM	Millimolar

MMA	Monomethylamine
nNOS	Neuronal Nitric Oxide Synthase
nM	Nanometers
NO	Nitric Oxide
NOS	Nitric Oxide Synthase
OD	Optical Density
p <	P-value
PAD	Peptidylarginine Deiminase
***Pa*DDAH**	*Pseudomonas Aeruginosa*
pan-NOS	Nitric Oxide Synthase Inhivitor
PBS	Phosphate Buffered Saline
pH	Potential Of Hydrogen - Scale
PPE	Personal Protective Equipment
PRMT	Protein Arginine Methyltransferases
qToF	Quadrapole Time Of Flight
RT-PCR	Reverse Transcription Polymerase Chain Reaction
R2	Coefficient of Determination
RPM	Rotation Per Minute
SAM	S-Adenosine Methionine
SD/ STD	Standard Deviation
SDMA	Symmetric Dimethylarginine
SDS	Sodium Dodecyl Sulphate
SDS-PAGE	Sodium Dodecyl Sulphate Polyacrylamide Gel Electrophoresis
SEM	Standard Error of The Mean
siRNA	Small Interfering RNA

sp^2	One S Orbital and Two P Orbitals Hybridize
StrB1	L-Arginine:Inosamine-Phosphate Amidinotransferase
TBS	Tris Buffered Saline
TBST	Tris Buffered Saline-Tween
ToF	Time-Of-Flight
UPLC-MS	Ultra-Performance Liquid Chromatography – Mass Spectrometry
µg	Microgram
µL	Microliter
µM	Micromole
V_{max}	Maximum Velocity of The Reaction
ZIR26	Small Molecule Inhibitors
ZST152	Small Molecule Inhibitors
ZST316	Small Molecule Inhibitors
$t_{1/2}$	Time Half-Life
v/v	Volume Per Volume
w/v	Weight Per Volume

Chapter 1 – INTRODUCTION

1.1 Nitric Oxide

Nitric Oxide (NO) is a chemical entity constituted of oxygen and nitrogen linked by a double covalent bond, and the nitrogen atom lacks one electron in the sp^2 orbital, conferring NO a high reactivity towards different types of molecules. As NO is lipophilic and electrically neutral, it is capable of crossing biological membranes rapidly, but its half-life is limited to a few seconds due to its elevated reactivity (Picón-Pagès et al 2019).

NO is a gaseous signalling molecule (Liu, H, Weng & Yang 2017) that is produced by virtually all organisms, from bacteria to plants and animal cells. The signalling activity of NO is mediated by interactions with a variety of molecular targets. The enzyme soluble guanylate cyclase (sGC), which catalyses the conversion of GTP to cGMP, is one of the key molecular targets for NO signalling. NO activates the enzyme by binding to the heme core and this results in increased concentrations of cyclic GMP. The majority cGMP effects are mediated by the activation of the protein kinase G (PKG), which phosphorylates a variety of targets including the IP3 receptor, calcium, and potassium channels. As a result of these effects, calcium sequestration is increased, and intracellular calcium concentrations is reduced. PKG also stimulates myosin light chain (MLCP) activity and the combined effects of reduced calcium and increased MLCP activity results in vascular smooth muscle relaxation (Hanafy, Krumenacker & Murad 2001).

NO plays a crucial role in many biological processes, across different organ systems such as the immune system where it participates to defence against pathogens (Stuehr & Marletta 1985), the nervous system where it acts as a neurotransmitter (Esplugues 2002), the endocrine system where it regulates the release of several hormones, including vasopressin (Ota et al.

1993) and insulin (De Angelis Lobo D'Avila et al. 1999), respiratory system where it maintain the pulmonary vascular reactivity (Stamler et al. 1994), vision system where it regulates the retinal blood flow (Koss 1999), urogenital system where it is involved in the relaxation of urethra (Kawahara 1994) and detrusor muscle (Chung et al. 1996), excretory system where it controls renal vasodilation (Toda & Okamura 2011). However, the most studied context for nitric oxide physiological roles is within the cardiovascular system, where it is responsible for vasodilation and maintaining vascular tone, thus playing a key role in the regulation of blood pressure and blood flow (Figure 1) (Colasanti & Suzuki 2000; Röszer 2012; Rees et al. 1989). NO is also a key modulator of angiogenesis and neovascularisation (Cooke & Losordo 2002). NO inhibits endothelial cell apoptosis *via* inactivation of caspase-3 (Dimmeler et al. 1999; Rossig et al. 1999) and increases the expression of vascular endothelial growth factor (VEGF) or fibroblast growth factor, thus stimulating endothelial cell proliferation (Dulak et al. 2000; Ziche et al. 1997). Furthermore, NO suppresses the synthesis of the anti-angiogenic protein angiostatin (Matsunaga et al. 2002), enhances the expression of $\alpha_v\beta_3$ (Murohara et al. 1999) and upregulates the urokinase-type plasminogen activator *via* release of the basic fibroblast growth factor (Ziche et al. 1997). This favours extracellular matrix dissolution and endothelial cells migration (Ziche et al. 1997; Cooke & Losordo 2002).

However, its concentration needs to be maintained within a tight range, since any imbalance can result in pathological conditions, causing diseases associated with either insufficient NO, such as hypertension, atherosclerosis, blood vessels disease (Levine, Punihaole & Levine 2012), endothelial dysfunction (Picón-Pagès, Garcia-Buendia & Muñoz 2019) or excessive NO production, including septic shock, cancer, aberrant neovascularization, chronic inflammation (Luiking, Engelen & Deutz 2010) (Levine, Punihaole & Levine 2012).

Figure removed due to copyright restriction

Figure 1: Diagram showing the NO regulatory functions in the human body. Source: Journal of Geriatric Cardiology, 2011.

NO is synthesised from L-arginine via a reaction catalysed by the enzyme nitric oxide synthase (NOS). Three isoforms of NOS have been identified, each isoform exhibiting different tissue distribution (Leiper, J & Nandi 2011): neuronal (nNOS), its functions include synaptic plasticity in the central nervous system and smooth muscle relaxation; endothelial (eNOS), which mediates regulation of vasodilation and blood pressure among other roles; and inducible or inflammatory (iNOS), mostly found in immune cells, and induced by signalling pathways and cytokine production. The primary role of iNOS is to defend against pathogens, mediating cell death (Knott & Bossy-Wetzel 2009).

While NO modulates a significant number of physiological processes, under specific circumstances it can be converted into highly reactive and harmful molecules, including peroxynitrite ($ONOO^-$), metal-nitrosyl complexes and S-nitrosoglutathione (GSNO) that modify the function of proteins, DNA, and lipids (Knott & Bossy-Wetzel 2009; Habib & Ali 2011; Arora et al. 2016), leading to cell death and dysfunction of tissue (Opatrilova et al. 2018).

Excessive NO production is mainly caused by the inducible isoform of NOS, iNOS (Colasanti & Suzuki 2000), which contributes to the development of a variety of human diseases and pathological conditions, including cancer (Luanpitpong & Chanvorachote 2015), septic shock (Lambden 2019), arthritis (Yki-Järvinen, Bergholm & Leirisalo-Repo 2003), retinopathy and aberrant neovascularization (Cooke 2003) (Opatrilova et al. 2018).

Despite growing evidence about the potential therapeutic advantage in targeting excessive NO synthesis, there is no clinically available drug that inhibits this pathway (Leiper, J & Nandi 2011; Opatrilova et al. 2018). In addition, the double-edged nature of NO and its key role in human physiology and homeostasis makes developing treatments options targeting NO toxicity especially difficult.

Isoform and/or tissue selective inhibition of NOS have been proposed as a strategy to target excessive NO production without disrupting its physiological functions, but this has revealed to be particularly challenging (Zhang et al. 1997) due to a high degree of similarity among NOS isoforms. Several studies have been reported showing isoform selective NOS inhibition *in vitro* and in animal models, but neither these compounds nor pan-NOS inhibitors have progressed past clinical trial. Aminoguanidine was one of the first iNOS selective inhibitors to be reported and kinetically characterised (Wolff & Lubeskie 1995). This compound exhibited great therapeutic potential delaying disease onset and progression and improving survival and markers of disease in *in vitro* and *in vivo* models of a variety of pathological conditions including autoimmune diabetes (Corbett & McDaniel 1996), experimental allergic encephalomyelitis (Zhao et al. 1996), endotoxic (Wu et al. 1995) and haemorrhagic shock (Soliman 2014), oral mucositis (Leitão et al. 2007), methotrexate-induced hepatotoxicity and nephrotoxicity (Hafez et al. 2015), and diabetic retinopathy (Mishra & Newman 2012). Alderton et al. (2005) have identified some potent, time-dependent, competitive iNOS inhibitors (GW274150 and GW273629) exhibiting high selectivity against

eNOS and nNOS *in vitro*. Further experiments conducted in mice also confirmed the capacity of these compounds to inhibit LPS-induced elevation of plasma nitrate and nitrite levels, thus effectively inhibiting iNOS *in vivo* (Alderton et al. 2005). In addition, Granados et al. (2015) reported the efficacy of small-molecule pan-NOS and iNOS selective inhibitors in decreasing cell proliferation, migration, stem cell renewal and tumour growth and metastases in triple negative breast cancer, providing evidence for actual clinical relevance of NO inhibition in cancer (Granados-Principal et al. 2015). However, this proposed therapeutic approach has encountered several clinical trials fails (Bailey et al. 2007; Brindicci et al. 2009; Hoffmann & Goadsby 2012; Seymour et al. 2012; Singh & Dikshit 2007), and appears to have come to an end.

As an alternative to isoform-selective NOS inhibition, the indirect inhibition of NO overproduction by regulating DDAH activity and decreasing the metabolism of NOS inhibitors has emerged as a novel approach for treating pathological conditions related to excessive NO production.

1.2 Methylated Arginines

Arginine is a proteinogenic amino acid that plays a key role in a variety of biological pathways, and it is a precursor for the synthesis of proteins and other important biological molecules such as NO and dimethylarginine (Unlu et al. 2021). Endogenous arginine analogues known as asymmetrical methylated arginines inhibit all three NOS isoforms reversibly and competitively (Murphy et al. 2016). In eukaryotes, three types of methylated arginine have been identified: monomethyl L-arginine (L-NMMA); asymmetric dimethylarginine (ADMA); and symmetric dimethylarginine (SDMA) (Kakimoto & Akazawa 1970), with only ADMA and L-NMMA acting as direct NOS inhibitors. Although SDMA does not inhibit NO directly, it

competes with arginine transport by the y^+ cationic amino acid transporters, limiting arginine absorption into endothelial cells, thus reducing NO production indirectly (Kittel & Maas 2014).

Methylated arginines are released into the cytoplasm following the post-translational methylation of arginine residues incorporated into different proteins, which contributes to the diversity of protein function, and subsequent proteolysis (Kittel & Maas 2014). These reactions are catalysed by protein-arginine methyl transferase (PRMTs) enzymes, which allow the transfer of the methyl group from S-adenosine methionine (SAM) to the guanidine groups of arginine residues (Fulton, Brown & Zheng 2019). Nine different PRMTs have been reported with three different types of activity and among these type 1 PRMTs is associated with the production of ADMA and L-NMMA, while SDMA and L-NMMA are produced by type 2 PRMTs (Tain & Hsu 2017).

The catabolism and elimination of methylarginines was assumed first to occur exclusively by renal excretion (Kakimoto & Akazawa 1970). Further investigations have demonstrated the existence of a major metabolic pathway for the elimination of asymmetrically methylated arginine residues (L-NMMA and ADMA) by the enzyme dimethylarginine dimethylaminohydrolase (DDAH). Whereas SDMA was confirmed to be predominantly excreted through renal excretion, therefore representing an endogenous indication of renal function (Vallance, Patrick & Leiper 2004). ADMA and SDMA are also metabolised by alanine glyoxylate aminotransferase 2 (AGTX2), but this second pathway only contributes to less than 20% of the total elimination (Ogawa, T., Kimoto & Sasaoka 1990) (Figure 2).

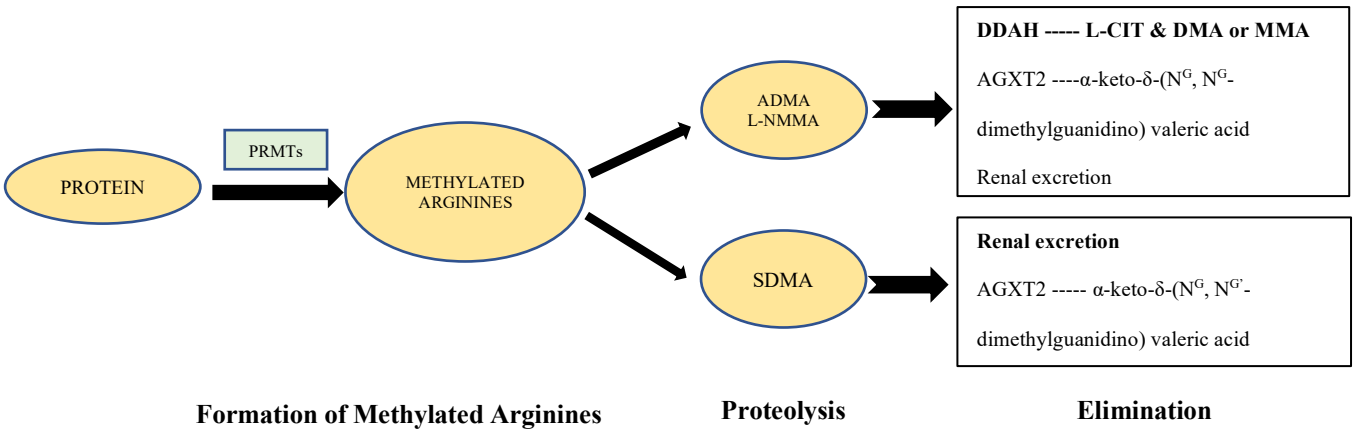

Figure 2: Representation of the life cycle of methylated arginine. Main metabolic pathway highlighted in bold font.

Circulating ADMA is found at greater concentrations than L-NMMA and is widely regarded as the primary inhibitor of NOS activity (Vallance, P. et al. 1992) and the only known posttranslational protein modification product with significant biological effects (Leiper, J & Nandi 2011). Since its discovery, many studies have been conducted on ADMA and the NO pathway demonstrating the correlation between changes in physiological ADMA concentrations and diseases. Increased ADMA levels are associated with conditions such as hypertension and cardiovascular disease (Liu, X et al. 2018), while low ADMA concentrations are observed in patients with sporadic form of amyotrophic lateral sclerosis (Isobe, Abe & Terayama 2010). As previously mentioned, ADMA is produced in most cells of the body daily and a small amount is eliminated by renal excretion, while the outstanding part is metabolised by the enzyme dimethylarginine dimethylaminohydrolase 1 (DDAH1) (see section 1.3).

The activity of the enzyme DDAH1, which metabolises methylarginines to L-citrulline (CIT) and methylamines, actively regulates ADMA concentrations *in vivo*. Inhibiting *h*DDAH1 activity would allow to achieve a targeted increase in ADMA concentrations and may provide a novel therapeutic target to treat diseases where excessive NO production is involved in the disease progression and associated with poor prognosis, such as septic shock, cancer, and aberrant neovascularisation. In this context, an indirect inhibition of NO synthesis through

*h*DDAH1 inhibition might favour the achievement of a fine modulation of NOS activity that represses NO overproduction without affecting its physiological roles. Thus, indirect inhibition of NOS via *h*DDAH1 would enable for more precise and selective control of NO concentrations.

1.3 Dimethylarginine Dimethylaminohydrolase 1 (DDAH1)

Historically, Ogawa et al. (1987) first reported a cytosolic enzyme that catalyses the metabolism of ADMA and L-NMMA, known as DDAH (Ogawa, Tadashi, Kimoto & Sasaoka 1987). The active site of DDAH shows a catalytic triad of Cys273, His172 and Asp126 which is associated with the conversion of ADMA or L-NMMA to CIT and is highly conserved across different species (Galkin et al. 2004; Murray-Rust et al. 2001; Palm et al. 2007). The finding by Tojo et al. (2000) that DDAH and NOS isoforms have distinct expression sites in blood vessels and the kidney (Tojo, Kimoto & Wilcox 2000), as well as that DDAH and NOS are co-expressed in cells (Tojo et al. 1997), identified that NO activity may also be regulated in a cell-specific manner by DDAH-induced changes in cellular ADMA concentration (Wilcken et al. 2007).

DDAH structure appears to be highly conserved across mammalian species such as sheep, mice, rats, and humans (Leiper, JM et al. 1999) and its expression differs little between foetal and adult tissues. Vallance, Leiper, and colleagues (1999) reported the presence of two isoforms of DDAH enzyme in mammals, DDAH1 and DDAH2, both supposedly responsible for the breakdown of ADMA and L-NMMA, thus playing an important role in maintaining NO homoeostasis (Leiper, JM et al. 1999). The chromosomal localization of the DDAH family of enzymes is consistent with gene amplification, and a comparison of the gene structures confirms that the intron/exon organisation is highly conserved (Tran et al. 2000). A phylogenetic analysis

of DDAH sequences from various species (figure 3) indicates that DDAH gene duplication occurred 400 million years ago, prior to the emergence of bony fish (Gillett et al. 1993, Tran et al. 2000).

According to a study by Tran and colleagues (2000), DDAH1 was found primarily in the brain, liver, and kidney, while DDAH2 was predominant in the heart, lung, kidney, and placenta (Tran et al. 2000). However, recent studies using more advanced techniques such as RT-PCR and immunohistochemistry have allowed the identification of new sites of expression and a characterization of the regional and cellular distribution of both isoforms (Hulin et al. 2020) (Kozlova et al. 2021). DDAH2 was first indicated to metabolise L-NMMA in 1999 by Leiper et al. Further studies have been conducted to analyse the metabolic activity of DDAH2 *in vivo*, and variations in ADMA concentration levels have been observed following DDAH2 knockdown in animal models. However, the metabolism of ADMA by DDAH2 *in vitro* failed to be reproduced and there is conflicting evidence about the actual role of this isoform in metabolising methylarginines directly (Hulin et al. 2020). Based on these considerations, this project will focus on the identification of novel DDAH1 inhibitors and DDAH2 will not be further explored in this study.

Frey et al. (2006) identified and crystallised the structure of DDAH1, highlighting different properties of the protein. The structure of DDAH1 showed a propeller-like fold that is comparable to other arginine-modifying enzymes, and a flexible loop that can take on many shapes and acts as a lid in the opening active site. The orientation and the way inhibitors interact with the active site can provide information about the enzyme's regulation and the molecular processes affected by its inhibition. Furthermore, the structural properties described can be used to guide the development of new DDAH1 modulators, which could be effective in the treatment of NOS dysfunction-related disorders (Frey et al. 2006).

Figure removed due to copyright restriction

Figure 3: Phylogenetic analysis of DDAH sequence indicating microbial and eukaryotic DDAH sequences (Tran et al. 2000).

1.4 Targeting the NO/ ADMA/ DDAH pathway

ADMA and L-NMMA are metabolised by *h*DDAH1 into CIT and dimethylamine (DMA) or monomethylamine (MMA), respectively (Ogawa, Tadashi, Kimoto & Sasaoka 1987). Following *h*DDAH1 inhibition, ADMA accumulates within the cell leading to the inhibition of NOS activity and consequently, blocking NO production (figure 4). This indicates that *h*DDAH1 is a crucial NO modulator.

Enhanced *h*DDAH1 expression has been linked to several pathological conditions and there is increasing evidence demonstrating its potential as a novel therapeutic target. Recent studies have shown the first indications of the therapeutic potential of *h*DDAH1 inhibition by small molecules in *in vitro* and *in vivo* models of endotoxic shock (Nandi et al. 2012; Wang et

al. 2014), pulmonary fibrosis (Pullamsetti et al. 2011), melanoma (Wang et al. 2014), prostate (Kami Reddy et al. 2019) and triple negative breast cancer (Hulin et al. 2019).

Nandi and colleagues (Nandi et al. 2012) provided the first proof-of-concept that both genetic and pharmacological suppression of DDAH1 activity exhibited improved cardiovascular haemodynamics and reduced circulatory collapse in two rodent models of endotoxic shock. This was further supported by the experiments performed by Wang et al. in 2014 (Wang et al., 2014), which demonstrated that pharmacological DDAH1 inhibition by L-257 was associated with preservation of organ function, prolonged survival, and improved cardiovascular haemodynamics in an *in vivo* model of septic shock. Pullamsetti et al. (2011) also identified that the pharmacological inhibition of DDAH1 by L-291 in mice affected by bleomycin-induced pulmonary fibrosis was linked to reduced collagen proliferation, lung cellular activity, and normalisation of lung function. This demonstrated the potential for DDAH1 inhibition to restore lung function and to be explored as a novel treatment for pulmonary fibrosis.

Wang et al. (2014) found that N5-(1-Imino-2-chloroethyl)-L-ornithine dihydrochloride (Cl-NIO), a powerful time and concentration-dependent covalent irreversible inactivator of *h*DDAH1, inhibited NO biosynthesis in melanoma cell lines. Furthermore, Kami Reddy et al. (2019) showed that incubation of prostate cancer cells with *h*DDAH1 inhibitors resulted in a decrease in NO production following ADMA accumulation and in the inhibition of cell proliferation. Also, DDAH1 inhibition was investigated *in vivo* in five groups of mice, screening three novel compounds (DD1E5, DD1C7 and DD1G7) and this demonstrated that DDAH1 inhibition reduced tumour growth by restraining tumour angiogenesis (Kami Reddy et al. 2019). Moreover, Hulin et al. demonstrated that *h*DDAH1 inhibition by siRNA, miRNA 193b-3p (Hulin et al. 2017) and by two small molecule inhibitors (ZST316 and ZST152) (Hulin et al. 2019) was able to suppress neovascularisation and cell migration in triple negative breast

cancer cell lines. The inhibition of *h*DDAH1, with consequent accumulation of ADMA, is also a promising strategy for suppressing traditional mechanisms of angiogenesis, as demonstrated by Fiedler and colleagues (Fiedler et al. 2009). In this study, increased ADMA concentrations suppressed VEGF-induced human umbilical vein endothelial cells migration, polarisation and focal adhesion turnover by inhibiting the Rac1-induced phosphorylation of vasodilator stimulated phosphoprotein (Fiedler at al. 2009).

The development of potent *h*DDAH1 inhibitors has the potential to target excessive NO synthesis more efficiently in those areas that overexpress this enzyme, such as cancer tissues, while preserving NO biological functions. This would pave the way for the development of a new generation of therapeutic agents.

Different classes of DDAH1 inhibitors have been synthesised over the last two decades. The first compound to be identified as mammalian DDAH1 inhibitor was S-nitrosohomocysteine (Hong & Fast, 2005). Only a few months later Rossiter and colleagues (Rossiter et al. 2005) published a structure activity relationship (SAR) study investigating the inhibitory potential of butanoic acid derivatives and arginine analogues as DDAH1 inhibitors, which identified the 2-methoxyethylic substituted arginine L257 and its methyl ester analogue L291 as two of the most potent and selective DDAH1 inhibitors (Rossiter et al. 2005). Another SAR study investigated amidine based DDAH1 inhibitors, but these molecules exhibited poor selectivity over NOS (Kotthaus et al. 2008). Different compounds with non-amino acid like structures, like ebselen (Linsky et al. 2011) and PD404182 (Ghebremariam et al. 2014), have also shown good *h*DDAH1 inhibition thanks to their ability to inactivate the catalytic cysteine residue, but these compounds presented many off target effects (Murphy et al 2016).

Despite the availability of several DDAH1 inhibitors (Murphy et al 2016), only a limited number of chemical structures have been investigated *in vivo* and they all exhibit high hydrophilicity, amino acid backbone and positive charge at physiological pH. These

characteristics are likely responsible for the low toxicity exhibited by these compounds but might impact on their pharmacokinetic profiling and limit therapeutic applications (i.e. limited blood brain barrier permeability).

A preliminary study performed within our group has demonstrated that the potent DDAH1 inhibitor ZST316 (K_i = 1 µM and IC_{50} = 3 µM) exhibits an encouraging toxicological profile. A group of 18 FVB mice were treated with ZST316 administered via intraperitoneal injection at the dose of 30 mg/Kg daily for 3 weeks and were sampled on day 21. Mice were monitored daily for any clinical sign of toxicity and distress, and body weight were recorded at least twice a week. The chronic treatment was well tolerated, no clinical signs of toxicity or distress were noticed, and the mouse body weight recorded during treatment was superimposable to that of untreated animals (Mangoni et al. 2022). Despite the promising toxicological results, it is not enough to exclude toxicity in different organ systems; therefore, additional extensive investigations with a particular focus on blood pressure effects in the cardiovascular system are needed before contemplating human administration,. Unfortunately, ZST316 also exhibited some undesirable pharmacokinetic properties, such as short half-life ($t_{1/2}$ = 6.06 h following a 30 mg/Kg intravenous administration), high first-pass metabolism and limited oral bioavailability (F% = 4.7and high levels of metabolites detected in the urine, following a 60 mg/Kg oral administration). Thus, the identification of novel DDAH1 inhibitors with diversified chemical scaffolds and pharmacokinetic profile is warranted.

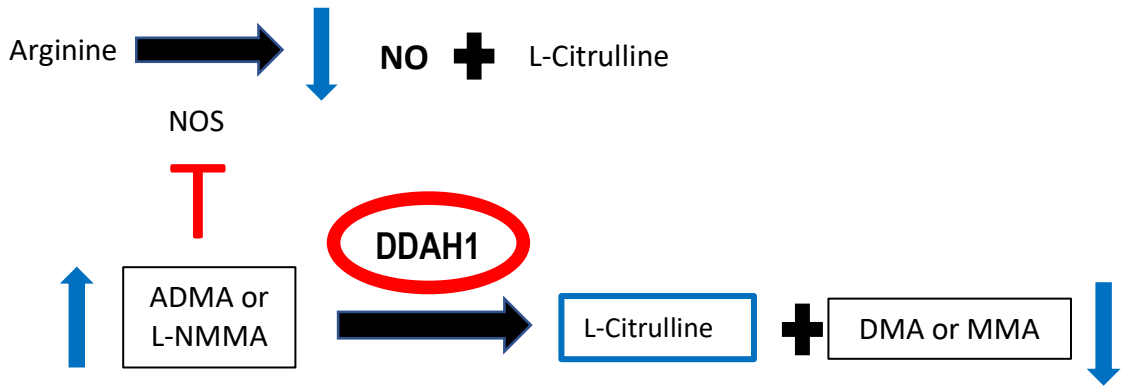

Figure 4: Representation of NO/ADMA/DDAH pathway.

1.5 Artificial Intelligence in drug discovery and development

Drug discovery is a complex, expensive, and time-consuming process, and for many years the pharmaceutical industry has been investigating innovative strategies to reduce costs and increase efficiency. Artificial Intelligence (AI) consists in the use of machine learning to power research and problem solving and it is being extensively applied to drug discovery worldwide (figure 5) (Chan et al. 2019). Artificial neural networks and deep learning algorithms provide exceptional support to structure- and ligand-based virtual screening, toxicity and physiochemical prediction, pharmacophore modelling, and quantitative structure–activity relationship, thus increasing the efficiency and reducing the time and costs associated with drug design and discovery (Carpenter & Huang 2018; Gupta et al. 2021). The application of AI algorithms to the screening of big databases of compounds might prove instrumental to the identification of novel DDAH1 inhibitors and their development into drug candidates for the treatment of diseases associated with excessive NO synthesis.

Figure removed due to copyright restriction

Figure 5: The applications of artificial intelligence (AI) in drug discovery. Source: Paul, D., et al. (2021). Drug discovery today, 26(1), 80–93 (Paul et al. 2021).

The American company Atomwise Inc. (Atomwise, 2021) specialises in using AI to develop a pipeline of small-molecule drug candidates to advance into preclinical studies.

Through a collaboration with this company, AI has been used to screen billions of existing compounds from different libraries against the crystal structure of DDAH1 and 70 small molecules have been identified as potential *h*DDAH1 inhibitors and ranked based on their predicted capability to bind to the enzyme active-site and their drug likeness.

Chapter 2 – AIMS OF THE PROJECT

2.1 Hypothesis & Aims

This project is focused on the hypothesis that novel *h*DDAH1 inhibitors can be identified either by the use of AI or by introducing targeted chemical modifications to the structure of existing inhibitors.

The aim of this study is to identify novel *h*DDAH1 inhibitors with the potential to be developed into new therapeutic agents. This will be achieved by developing a robust UPLC-MS based *h*DDAH1 activity assay that will allow to measure the capacity of HEK293T cell lysates overexpressing recombinant *h*DDAH1 to catalyse the metabolism of ADMA into CIT. This assay will then be used to measure the *in vitro* inhibitory potential of at least seven compounds: six of the 70 compounds designed by AI and one compound specifically designed within the Clinical Pharmacology lab using the known *h*DDAH1 inhibitor ZST316 (Tommasi et al, 2015; Hulin et al, 2019) as a template. This project will be divided into the following experimental objectives:

- Harvesting HEK293T cells stably overexpressing *h*DDAH1 and quantification of the total protein content of the cell lysate,
- Verification of expression of *h*DDAH1 lysate by Western Blot,
- Development and validation of the UPLC-MS method to measure *h*DDAH1 activity and characterisation of the kinetic behaviour of the *h*DDAH1 expression system,
- Screening of seven compounds: six molecules identified as potential *h*DDAH1 inhibitors by AI, and one molecule designed within the clinical pharmacology lab,

• Investigation of kinetics of *h*DDAH1 inhibition by these compounds and determination of the kinetic parameters, i.e., constant of inhibition (K_i) and half-maximal inhibitory concentration (IC_{50}).

2.2 Biotechnology significance

A study conducted by Tran et al. (2000) explored the evolutionary history of mammalian DDAH isoforms by searching several nucleotide and protein databases in order to identify novel DDAH-like sequences. The results of this study have identified that the six exons and intron/exon boundaries that comprise the coding region of both DDAH isoforms are highly conserved across species, especially in mammals and that DDAH-like sequences are encountered in the fruit fly, *Drosophila melanogaster*, and the zebrafish, *Danio rerio* (Tran et al. 2000). The same group had previously identified genes encoding for proteins analogous to DDAH in the genome of several microbes (Santa Maria et al. 1999), including *Streptomyces coelicolor*, and the pathogens *Pseudomonas aeruginosa* and *Mycobacterium tuberculosis*, with *S. coelicolor* exhibiting the highest level of homology. Functional similarity between these enzymes and human DDAH was also confirmed by demonstrating the capacity of these DDAH-like protein to metabolise methylated arginines. These findings further support the crucial role of DDAH in arginine metabolism and are particularly significant when considering that these microbial species do not express NOS, indicating that DDAH might have other roles in bacteria (Santa Maria et al. 1999). Better understanding of these roles and the development of bacteria selective DDAH inhibitors might open the way to the discovery of novel classes of anti-microbial drugs (Kotthaus et al. 2008). DDAH also exhibits high levels of structural homology with other enzymes involved in arginine metabolism, such as the enzyme Arginine:glycine amidinotransferase (AGAT) (Humm et al. 1997), and L-Arginine:inosamine-phosphate

amidinotransferase (StrB1) (Fritsche et al. 1998). Furthermore, despite low homology when comparing the whole aminoacidic sequence, DDAH active site shares distinct similarities with that of peptidylarginine deiminase (PAD) (Stone et al. 2005).

The discovery that the DDAH gene is evolutionarily well conserved suggests that the enzyme provides a significant survival advantage. The bacterial isoform of DDAH found in *Pseudomonas aeruginosa* (*Pa*DDAH) has been extensively investigated to gain better understanding of the regulatory and molecular mechanisms involved in methylarginine utilisation in bacteria (Lundgren et al. 2017) and for the identification of potential modulators of the enzyme activity in bacteria, as well as in other species thanks to the highly conserved structure of these enzymes (Frey et al. 2006). The existence of two DDAH isoforms in mammals with distinct tissue distributions suggests that the regulation of methylarginine concentration is of significant biological importance, and a highly conserved DDAH sequences in divergent species as microbes and mammals, indicates that asymmetric methylarginine residue metabolism precedes the evolution of NOS enzymes. The development of reversible DDAH inhibitors is not only important for therapeutic purposes, but also to investigate the role and the importance of DDAH in other species.

Another important aspect of biotechnological significance of the proposed research is the use of biotechnological techniques to overexpress *h*DDAH1 in human embryonic kidney-derived epithelial cells HEK293. DDAH1-expressing HEK293T cell lysate was used as a source of the enzyme in all the *in vitro* experiments hereby discussed. The major component of biotechnological significance is the application of AI to drug discovery. As previously mentioned (chapter 1.5), AI represents a state-of-the-art technique that can be used to develop enzyme inhibitors by using machine learning to power research and drug discovery and development. Using advanced technological techniques like AI and UPLC-MS, this project represents a steppingstone to leverage for the development of novel DDAH1 modulators with

potential therapeutic application for treatment of conditions like cancer and inflammatory diseases.

In summary, the NO/DDAH/ADMA pathway has been proposed as a potential therapeutic target to treat diseases caused by excessive NO, such as septic shock and cancer (Hulin et al. 2020; Leiper, J & Nandi 2011) and the development of novel DDAH1 inhibitors is a future perspective to investigate the importance of DDAH in other species.

2.3 Proposed research

As mentioned in section 1.4, inhibiting *h*DDAH1 to increase ADMA concentrations and thus modulate NOS activity is a promising pharmacological approach to reduce excessive NO concentrations. Hence, this project is focused on the identification of novel *h*DDAH1 inhibitors with potential therapeutic applications in the treatment of conditions associated with excessive NO synthesis. It is hypothesised that at least one of the seven screened compounds would act as a *h*DDAH1 inhibitor with a K_i <10 μM and/or an IC_{50} < 20 μM.

Due to the intellectual agreement between the Department of Clinical Pharmacology and Atomwise, the chemical structure of the potential inhibitors is unknown to our group and thus will not be reported.

Chapter 3 - MATERIALS & METHODS

3.1 Research facilities

For the whole duration of this project, the experiments were conducted in the Department of Clinical Pharmacology, Flinders Medical Centre. All procedures involving cell culture were conducted in the tissue culture room as described in section 3.3.1. Proteomics Facility was used to analyse colorimetric protein assays according to section 3.3.2. Also, during this project, all safety precautions were carried out according to Flinders University Work Health and Safety directives, including the use of the appropriate personal protective equipment (PPE).

3.2 Materials and equipment

Materials and reagents used during this project, were purchased commercially, used, and stored precisely as indicated by the accompanying information and safety data sheets, and are listed according to table 1. Chemicals and reagents utilised were of analytical grade, while all solvents used in this project were of MS-grade (Table 1). Detailed reagent compositions and preparation protocols for media, solutions and buffers are specified in Appendix A – Solution preparation and equipment, consumables and software used are listed in Appendix B – Equipment, Consumables and Software, (table 8).

Table 1: List of used materials, reagents, and antibodies.

REAGENTS AND SOLVENTS	SUPPLIER
2-propanol	Merck, NSW, Australia
Acetic Acid	Chem Supply, SA, Australia
Acetonitrile	Merck, NSW, Australia

Acrylamide/Bis 40% Solution 37.5:1	Bio-Rad Laboratories, CA, USA
Ammonium persulphate (APS)	Sigma-Aldrich, MO, USA
Bovine Serum Albumin (BSA)	Sigma-Aldrich, MO, USA
cOmplete™ Protease Inhibitor Cocktail (Roche)	Sigma-Aldrich, MO, USA
Coomassie Brilliant Blue G-250	Bio-Rad Laboratories, CA, USA
Copper sulphate	Chem Supply, SA, Australia
Dimethyl Sulfoxide (DMSO)	Merck, NSW, Australia
Dulbecco's Modified Eagle's Medium (DMEM)	Gibco, Life Technologies, VIC, Australia
Ethanol	Chem Supply, SA, Australia
EZQ protein quantification reagent	ThermoFisher Scientific, VIC, Australia
Foetal Bovine Serum (FBS)	Scientifix, VIC, Australia
Folin and Ciocalteu's Phenol	Merck, NSW, Australia
Formic acid	ThermoFisher Scientific, VIC, Australia
Glycine	Sigma-Aldrich, MO, USA
Hydrochloric Acid (HCl)	Sigma-Aldrich, MO, USA
L-citrulline (CIT)	Sigma-Aldrich, MO, USA
L-citrulline-d6 (CITd-6)	Toronto Research Chemicals, Canada
MEM non-essential amino acids	Gibco, Life Technologies, VIC, Australia
Methanol	Merck, NSW, Australia
Molecular markers - ColorBurst	Sigma-Aldirich, MO, USA
N,N,N′,N′-Tetramethylethylenediamine (TEMED)	Sigma-Aldrich, MO, USA
N^G, N^G-Dimethylarginine dihydrochloride (ADMA)	Sigma-Aldrich, MO, USA
Ovalbumin	ThermoFisher Scientific, VIC, Australia
Phosphate Buffered Saline (PBS) (1x)	Refer to Appendix A
Potassium phosphate 0.1 M	Refer to Appendix A
Puromycin	Sigma-Aldrich, MO, USA
Quick Start™ Bradford 1x Dye Reagent	Bio-Rad Laboratories, CA, USA
SDS sample buffer	Refer to Appendix A
Skim milk powder	Woolworths, SA, Australia
Sodium Bicarbonate (NaHCO3)	Chem Supply, SA, Australia
Sodium Carbonate (Na_2CO3)	Chem Supply, SA, Australia

Sodium Chloride (NaCl)	Chem Supply, SA, Australia
Sodium Dodecyl Sulfate (SDS)	Astral Scientific, NSW, Australia
Sodium Hydroxide (NaOH)	Chem Supply, SA, Australia
Sodium Pyruvate	Gibco, Life Technologies, VIC, Australia
Sodium Tartrate ($Na_2C_4H_4O_6 \cdot 2H_2O$)	Chem Supply, SA, Australia
SuperSignal West Pico chemiluminescent (ECL) HRP substrate	ThermoFisher Scientific, VIC, Australia
Tris base	Sigma-Aldrich, MO, USA
Tween® 20	ThermoFisher Scientific, VIC, Australia
ANTIBODIES AND INHIBITORS	**SUPPLIER**
Goat anti-DDAH1 primary antibody (ab22301) (1:2000)	Abcam, Cambridge, UK
HRP-conjugated Donkey anti-Mouse secondary antibody (1:2000)	FMC – Proteomic facility, SA, Australia
HRP-conjugated Rabbit anti-Goat secondary (ab6741) antibody (1:2000)	Abcam, Cambridge, UK
Mouse anti-FLAG primary antibody (F1804) (1:2000)	Sigma-Aldrich, MO, USA
Inhibitor candidates (A01-F01)	Atomwise, CA, USA
ZIR26	Clinical Pharmacology Department, FMC, Australia
ZST316	Clinical Pharmacology Department, FMC, Australia

3.2.1 Cell line

A stable cell line overexpressing *h*DDAH1 was already available within the Department of Clinical Pharmacology and was used in this project. *h*DDAH1 overexpression was achieved by Dr Sara Tommasi in a human embryonic kidney cell line, HEK293T. The decision to use this cell line was influenced by several factors. HEK293T cells grow effortlessly , reproduce quickly, and are extremely efficient at protein production (Dumont et al. 2016; Swiech, Picanço-Castro & Covas 2012; Thomas & Smart 2005). Despite the preparation of cell line was

not part of this project, the description of how this was achieved is briefly described in section 3.2.1.1.

3.2.1.1 Preparation of the stable cell line

The *h*DDAH1 open reading frame was included in pEF-IRES-Puro(6) vector which is suitable for mammalian expression as it contains the constitutively active elongation factor 1α promoter (EF1α). This vector allows for the generation of stably transfected eukaryotic cells due to the presence of *pac* gene encoding for puromycin N-acetyl-transferase, a protein able to confer resistance to the eukaryotic antibiotic puromycin. HEK293T cells were transfected with the pEF-IRES-DDAH-1 expression construct (4 μg) using Lipofectamine2000 in OptiMEM (Invitrogen, CA, USA) and cultured in complete DMEM medium supplemented with puromycin (1 μg/mL), to select stable transfectants, enabling only those cells to survive and grow in this environment.

3.3 Methodologies

3.3.1 Cell culture treatment

3.3.1.1 Maintenance of cells

Experiments involving the use of HEK293T cells overexpressing *h*DDAH1 enzyme were performed under sterile conditions using a tissue culture hood. All equipment and consumables were sterilised with 70% ethanol prior to use. Cells cultures were grown in complete Dulbecco's Modified Eagle's Medium (DMEM) supplemented with 10% foetal bovine serum (FBS) and containing antibiotic puromycin (1 μg/mL), using T175 flasks. Detailed formulation of the culture medium is provided in the Appendix A – Solution

preparation. Cell cultures were maintained in a humidified incubator at 37˚ C with 5% CO_2 until 95% confluence prior to passaging. The media was replaced every other day or as needed. Cells confluency and contamination were monitored regularly, using microscope Olympus CK2. A 12 wells plate was seeded with serum, incomplete and complete medium (DMEM) to monitor for possible contamination. Detailed media composition (complete and incomplete) is specified in Appendix A – Solution preparation. Cells were passaged in growth phase at ratio 1:5 using new T175 flasks, aspirating exhausted medium and cell debris, followed by the addition of complete DMEM and resuspending by pipetting up and down slowly until all cells were detached from the bottom of the flask. Cells were then, incubated in a humidified incubator according to the conditions described above.

3.3.1.2 Preparation of cell lysate

Each cell lysate batch was prepared from the pooled content of 12 x T175 flasks of 95% confluent HEK293T cells overexpressing *h*DDAH1. Cells were re-suspended in culture medium and centrifuged (3000 x RPM for 10 minutes at 4º C). The supernatant was discarded, and the pellet was washed twice with sterile phosphate buffered saline (PBS) and then, centrifuged in the same conditions. Detailed formulation of PBS is provided in the Appendix A – Solution preparation. Again, the supernatant was discarded, and pellet re-suspended into 0.1 M Phosphate buffer (pH = 7.4) and moved onto an ice-bath to prevent protein degradation and loss of enzymatic activity. Detailed formulation of the phosphate buffer is provided in the Appendix A – Solution preparation. Protein degradation was stopped by the addition of a proteinase inhibitor cocktail (50x) (Roche). Cell lysis was achieved by sonication (pulse = 1 second, cooling = 30 seconds and 40% amplitude), using SONICS equipment and the homogenates centrifuged (15000 x RPM for 10 minutes at 4º C) to separate the cell lysate from cellular debris. In this project, two batches of cell lysate were prepared from the same cell line

overexpressing *h*DDAH1 and hereby referred as HEK293T DDAH1 untagged preparation 1 and 2.

3.3.1.3 Preparation of cell lysate frozen stocks

Cell lysates and pellets were stored in 0.5 mL aliquots at -20º C immediately after preparation and for up to 6 months, then moved to the -80º C freezer for long-term storage. For each of the experiments reported in this project a fresh aliquot of lysate was used to minimise protein loss due to repeated freeze-thaw cycles.

3.3.2 Colorimetric protein assays

3.3.2.1 Lowry assay

The total protein concentration was determined using the Lowry assay, which is based on the principle that divalent copper ion forms a complex with peptide bonds under alkaline conditions and is reduced to a monovalent ion (Shen 2019). Once monovalent copper ion reacts with Folin reagent, it produces a blue compound with an optical density at 660 nm (OD_{660}) proportional to the amount of protein in each sample (Lowry et al. 1951). Lowry assay was chosen because it is inexpensive, easy to perform and generally associated with high sensitivity and precision. The Lowry reagent was prepared in a ratio 100:1:1 mixing three different solutions:

- Lowry A: containing a diluted alkaline solution with 0.4% sodium hydroxide (w/v) and 3% sodium carbonate (w/v) in water.
- Lowry B: containing an aqueous solution of 4% sodium tartrate (w/v) in water.
- Lowry C: containing an aqueous solution of 2% copper sulphate (w/v) in water.

Folin and Ciocalteu's Phenol Reagent was prepared in a ratio 1:1 in distilled water and protected from light due to its light-sensitivity. A standard curve utilizing, bovine serum albumin (BSA) standards (10, 25, 50, 75 µg) was prepared, and a 1:10 dilution in distilled water

was obtained for the samples with unknown protein concentration (*h*DDAH1 lysates). A volume of 25 µL of each diluted sample was added to distilled water to a final volume of 500 µL. Standards and samples were prepared in triplicate in borosilicate glass tubes. To every standard and unknown protein reaction mixture 2 mL of Lowry reagent was added and the reactions were incubated for 10 minutes at room temperature, followed by the addition of 250 µL of Folin and Ciocalteu's Phenol Reagent to each tube, vortex mixing and a further incubation for 15 minutes at room temperature. The OD_{660} was measured for each sample and standard and the calibration curve was obtained plotting the mean OD_{660} of each standard versus the corresponding amount of protein and was calculated according to the equation below.

Protein concentration = dilution factor x absorbance / slope x (1/ sample vol)

*Where the usual values are: dilution factor = 10, sample vol = 25.

3.3.2.2 Bradford assay

Another method used to determine protein concentrations was the Bradford assay, originally developed by Marion M. Bradford in 1976 (Bradford 1976). This method involves the binding of the dye (Coomassie Brilliant Blue G-250) to proteins, resulting in a shift of the absorption maximum of the dye from 465 to 595 nm. The increase in absorption at 595 nm is measured (Aminian et al. 2013). A standard curve utilizing BSA standards (0.05, 0.1, 0.2, 0.4, 0.6, 0.8, 1 mg/mL) was obtained, and the samples with unknown protein concentration (*h*DDAH1 lysates) were subjected to dilution in a range between 1:5 and 1:40. Standards and samples were prepared in triplicate in borosilicate glass tubes and a volume of 25 µL was added to 500 µL of dye reagent, then samples and standards were vortex mixed and incubated at room temperature for 5 minutes. A volume of 0.5 mL of each prepared solution was transferred into each well of a 96 well-plate. The absorbance at 595 nm was measured for each sample and standard utilizing the SpectraMax iD5 reader (Flinders University Proteomic Facility), and a calibration curve and corresponding equation were obtained by plotting the mean OD_{595} of each

standard versus the corresponding protein concentration (mg/mL). The best method of interpolation of the data (linear *versus* curvilinear regression) was chosen by comparing the coefficients of determination (R^2). The equation that best described the entire set of standard points was the one with the highest value of R^2.

3.3.2.3 EZQ assay

EZQ assay of ovalbumin (Weist et al. 2008), a fluorescence-based protein assay that facilitates fast quantitation of protein samples, was also used to determine the protein concentrations. A dilution series of ovalbumin standards was prepared (0.02, 0.05, 0.1, 0.2, 0.5, 1, 2 mg/mL) and a standard curve was obtained. The samples with unknown protein concentration (*h*DDAH1 lysates) were diluted in a range between 1:5 and 1:40. The assay was performed spotting 2 µL of protein sample, blank and standard onto a pre-cut sheet of Grade 5 Whatman paper, in triplicate. The proteins were fixed onto the paper by incubating with 40 mL of methanol and stirring at 50RPM for 5 min, then the paper was dried on low heat, followed by the addition of 35 mL of EZQ Protein Quantification Reagent stain (ThermoFisher Scientific) with stirring for 30 minutes. The paper was then, washed with 40 mL of EZQ destain (3 x 2 min with stirring, please refer to Appendix A – Solution preparation for the destain composition). Paper was imaged using the EZ-Doc Imager (Bio-Rad, Australia). Analyses was conducted using the software ImageLab, then data was exported to excel spreadsheet using the "EZQ Analysis Template – Manual Calculations" function. The standard equation was derived according to the equation below.

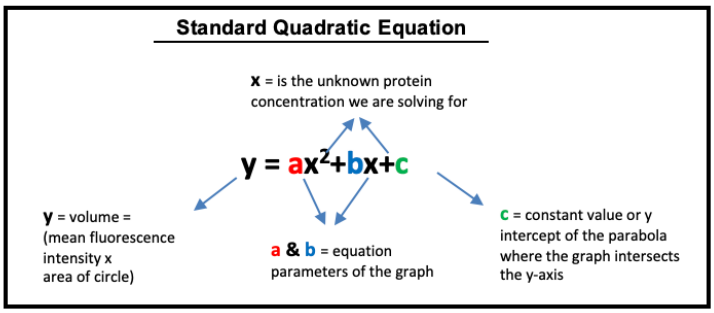

3.3.3 Western blot analysis

Qualitative western blot analysis was performed to confirm the presence of the protein of interest (*h*DDAH1) in the corresponding lysates.

A total of 6 samples were prepared by mixing 30 µg of total protein to 4 µL of 5 x SDS sample buffer and water to a total volume of 20 µL. Detailed formulation of SDS sample buffer is provided in the Appendix A – Solution preparation. Samples were denatured at 95° C for 5 minutes and then separated by SDS-PAGE. Denatured total proteins and molecular markers (220 kDa, ColorBurst; Sigma-Aldrich, Australia) were loaded onto two 4-10% polyacrylamide gels and run at 60 V until they passed through the stacking gels. Samples were then separated on 10% polyacrylamide running gels at 120 V and transferred to two Trans-blot nitrocellulose membranes (BIORAD; 0.45 µm) at 100 V for 1 hour (4° C) with stirring. Membranes were initially washed in Tris-buffered saline with 0.1% Tween® 20 detergent (TBST) (3 x 2 min) to remove any residual methanol that might contribute to background staining. Detailed formulation of TBST is provided in the Appendix A – Solution preparation. They were then blocked in a solution of 4% (w/v) non-fat dry milk in TBST overnight at 4º C, followed by incubation at room temperature for 90 minutes on a shaker, and a brief rinsing in TBST. Blot 1 was probed with goat anti-DDAH1 primary antibody (1:2000, Abcam; ab22301) and blot 2 was probed with mouse anti-FLAG primary antibody (1:2000, Sigma F1804) for 2 hr. Both

membranes were then washed in TBST (3 x 10 minutes with shaking) before incubation with the corresponding secondary antibody. Blot 1 was probed with HRP-conjugated Rabbit anti-Goat secondary antibody (1:2000, Abcam, ab6741) and blot 2 with HRP-conjugated Donkey anti-Mouse secondary antibody (1:2000, provided by the Flinders University Proteomics Facility) for 1 hour at room temperature.

Blots were treated with enhanced SuperSignal West Pico chemiluminescent (ECL) HRP substrate (Thermo Fisher Scientific) and imaged using a ChemiDoc Touch Imaging System (Bio-Rad, Australia). Previously characterised *h*DDAH1 cell lysates were used as positive control, while untransfected HEK293T cell lysate and FLAG DDAH2 expressing HEK293T cell lysate were used as negative control. The formulation of gels and buffers used in these experiments is available in the Appendix A – Solution preparation.

3.3.4 *h*DDAH1 activity assay

A Ultra-Performance Liquid Chromatography coupled to Mass Spectrometry (UPLC-MS) based assay was developed and validated to measure the enzyme activity in *h*DDAH1 overexpressing HEK293T cell lysates. This assay was developed by adapting a method previously reported by our group (Hulin et al. 2017; Tommasi, S. et al. 2017) and was used to measure the inhibitory potential of seven novel compounds.

3.3.4.1 UPLC-MS analysis

UPLC is an analytical technique that allows the separation of the analytes of interest from a complex matrix by using the flow of a selected solvent (recognised as the mobile phase) at increased pressure through a chromatographic column containing a stationary phase with specific chemical properties (Zhu et al. 2020). Mass spectrometry (MS) allows the detection

and quantification of said analytes based on the mass over charge ratio of the particles of which the substance is made of. This significant approach has a wide variety of applications due to its sensitivity, precision and selectivity (Lawson et al. 2017).

A UPLC-MS method was used to measure CIT formation from ADMA. CIT analysis was performed on a Waters ACQUITY Ultra Performance LC™ system coupled to a Waters Premier quadrapole time of flight (qToF) mass spectrometer with an electrospray ionisation source operated in positive ionisation mode. Time-of-flight (ToF) data were collected in MS mode between 100 and 500 Da with an instrument scan time of 0.5 seconds and inter-scan delay of 0.05 seconds. The MS parameters are shown in Table 2. Instrument control, data acquisition and data processing were performed using Waters MassLynx version 4.1 software. CIT was separated on a Waters Atlantis HILIC column (3 µm, 2.1 mm x 150 mm). The mobile phase comprised acetonitrile containing 0.1% v/v formic acid (mobile phase A) and 0.1% formic acid in a solution of 10 % v/v acetonitrile in water (mobile phase B) at a flow rate of 0.4 mL/min. Initial conditions were 95% mobile phase A, 5% mobile phase B. The proportion of mobile phase B was increased linearly to 69% over 11 minutes then returned to 5% for 2 minutes to re-establish equilibrium before injecting the next sample for analysis. The total duration of each chromatographic run was 15 minutes and samples were maintained at 15° C in the auto-sampler prior to analysis.

Selected ion chromatograms were extracted from the total ion chromatogram at m/z 176.10→159.14 and 181.13→165.17 corresponding to the fragments of CIT and citrulline-d6 (CIT-d6), respectively. CIT-d6 was used as an internal standard (IS) to correct for random and systematic errors in sample preparation, chromatography, and detection.

The method validation comprised the assessment of linearity, reproducibility (instrument precision, method precision, intra-day and inter-day assay precision and accuracy), and sensitivity (lower limit of detection or LLOD and lower limit of quantification or LLOQ).

Table 2: Mass spectrometer instrument settings.

Instrument Parameter	Setting
Capillary voltage (kV)	3.0
Sampling cone voltage (eV)	24.0
Extraction cone voltage (eV)	5.0
Source temperature (°C)	100
Desolvation temperature (°C)	300
Cone gas flow(L/Hr)	30.0
Desolvation gas flow (L/Hr)	400.0
Collision energy	5.0
Collision Cell Entrance	2.0
Collision Exit	-10.0
Collision Gas Flow (mL/min)	0.6

3.3.4.2 Preparation of standards

The incubation matrix comprised of *h*DDAH1-expressing HEK293T cell lysate (0.05 mg/mL), phosphate buffer (0.1 M, pH 7.4), DMSO (1 µL) and ADMA (100 µM). To prepare the standard solutions, the incubation matrix was spiked with 10 µL of CIT aqueous working solutions in the range of 20-100 µM (to obtain a final dilution of 1:10), giving six calibration standards into the range 2-10 µM in a total volume of 0.1 mL. The calibration curve included also a blank and a zero standard sample (processed with IS). Standards were extracted and reconstituted in the same manner as incubation samples (please refer to paragraph 3.3.4.3 for details). Calibration curves were obtained by plotting the peak area ratio CIT to IS versus the standard concentration and the resulting equation was used to quantify the concentration of CIT in incubation samples.

Calibrators were run at the beginning and at the end of every mass spectrometer run to ensure that the instrument performed consistently.

3.3.4.3 *h*DDAH1 activity assay – general method

Working solutions of each inhibitor were prepared in DMSO and 1 µL of the corresponding working solution in the range of 0-10,000 µM was included into each incubation mixture to obtain a final dilution of 1:100. Each incubation mixture and each calibrator contained a total solvent concentration of 1% DMSO, which does not affect *h*DDAH1 kinetic behaviour based on experiments previously conducted within our lab (unpublished data). Incubation mixtures were prepared in 12x75 mm borosilicate glass tubes and contained water, *h*DDAH1-expressing HEK293T cell lysate (0-0.08 mg/mL), phosphate buffer (0.1 M, pH 7.4), ADMA (0 – 1000 µM) and the potential inhibitor (0 -100 µM) in a total volume of 0.1 mL. The samples were prepared by adding in order: the potential inhibitor, water, phosphate buffer, and the protein lysate, then vortex mixed and cooled on ice until they were transferred into a water bath for incubation. Following a 5-minute pre-incubation step at 37º C with gentle shaking, reactions were initiated by the addition of the substrate (ADMA) and incubated at the same temperature for the time required by the specific experiment (0 – 60 minutes). Incubation reactions were terminated by the addition of 300 µL 0.1% formic acid in 2-propanol and 10 µL of the assay IS (50 µM CIT-d6). The samples were vortex mixed for 20 seconds and cooled on ice for 10 minutes prior to centrifugation (5 minutes at 18,000 x g) to precipitate the proteins. The supernatant (300 µL) was transferred to clean 12x75 mm borosilicate glass tubes and the solvent was removed by evaporation in a MiVac concentrator (T=50ºC, P=30 mbar, -OH programme, 30 minutes). The residue was redissolved in 125 µL of a 1:4 water/ 0.1% formic acid in 2-propanol mixture and a 5 µL aliquot was injected onto the UPLC column for analysis.

3.3.4.4 Protein linearity

The direct proportionality between *h*DDAH1 protein concentration and the amount of CIT formed for each reaction was verified through a protein linearity experiment, in which incubation time and substrate concentrations were maintained constant, while CIT concentration was plotted against the enzyme concentration. CIT formation was determined at 37º C in a total incubation volume of 0.1 mL. Incubation mixtures comprised of water, *h*DDAH1-expressing HEK293T cell lysate (0, 0.25, 0.5, 0.75, or 1 mg/ml), phosphate buffer (0.1 M, pH 7.4), DMSO (1µL) and ADMA (50 µM in one set of data and 500 µM in the other). Following pre-incubation at 37 ºC for 5 minutes, reactions were initiated by the addition of substrate (ADMA). After 50 minutes incubation, reactions were terminated and CIT extracted, reconstituted, and analysed as described in paragraph 3.3.4.3. Protein linearity was assessed over three independent experiments. Graphical representation of experimental data was obtained using GraphPad Prism (version 9.0 for Windows: GraphPad Software, San Diego, California USA).

3.3.4.5 Time linearity

The mathematical relationship between incubation time and the amount of CIT formed for each reaction was determined through a time linearity experiment, in which the enzyme and substrate concentrations were maintained constant, while incubation time was progressively increased. CIT formation was determined at 37 ºC in a total incubation volume of 0.1 mL. Incubation mixtures comprised of water, *h*DDAH1-expressing HEK293T cell lysate (0.5 mg/mL), phosphate buffer (0.1 M, pH 7.4), DMSO (1 µL) and ADMA (50 µM in one set of data and 500 µM in the other). Following pre-incubation at 37 ºC for 5 minutes, reactions were initiated by the addition of substrate (ADMA). The reactions were terminated at different incubation times (0, 20, 40, 60, 80 minutes) and CIT extracted, reconstituted, and analysed as

described in paragraph 3.3.4.3. Time linearity was assessed over three independent experiments. Graphical representation of experimental data was obtained using GraphPad Prism (version 9.0 for Windows: GraphPad Software, San Diego, California USA).

3.3.4.6 Determination of kinetic parameters K_m and V_{max}

The kinetics of ADMA metabolism to CIT by recombinant *h*DDAH1 overexpressed in HEK293T cells was then characterised and the kinetic parameters K_m and V_{max} derived. CIT formation was determined at 37º C in a total incubation volume of 0.1 mL. Incubation mixtures contained *h*DDAH1-expressing HEK293T cell lysate (0.5 mg/mL), phosphate buffer (0.1 M, pH 7.4), DMSO (1 µL) and ADMA (0 - 600 µM). Following pre-incubation (5 minutes), reactions were initiated by the addition of substrate (ADMA). After a 60-minute incubation, reactions were terminated and CIT extracted, reconstituted, and analysed as described in paragraph 3.3.4.3.

The enzyme activity was determined by measuring the rate of L-CIT formation and kinetic data are the mean of three separate experiments performed in singlicate. Graphical representation of experimental data was obtained using GraphPad Prism (version 9.0 for Windows: GraphPad Software, San Diego, California USA). An Eadie-Hofstee plot was also reported, but only used to aid visual representation of linearised data and the kinetic parameters K_m and V_{max}.

3.3.5 Screening of potential novel *h*DDAH1 inhibitors

*h*DDAH1 inhibitor candidates were screened based on their capacity to interfere with the rate of CIT formation in incubation reactions in which the enzyme and substrate concentration and incubation time were maintained constant. CIT formation was determined at 37º C in a total incubation volume of 0.1 mL. Incubation mixtures comprised of *h*DDAH1-expressing HEK293T cell lysate (0.5 mg/mL), phosphate buffer (0.1 M, pH 7.4), DMSO (1 µL), ADMA (100 µM), and *h*DDAH1inhibitor candidate (**A01**, **B01**, **C01**, **D01**, **E01**, **F01**; provided by Atomwise, and ZIR26; supplied by the Department of Clinical Pharmacology at Flinders University; each at five different concentrations in the range 0-100 µM). The well-characterised *h*DDAH1 inhibitor ZST316 (Murphy et al. 2016; Tommasi, Sara et al. 2015) was provided by the Department of Clinical Pharmacology at Flinders University and used as a positive control for the enzyme inhibition at the concentrations of 0.1 and 1 µM. Following a 5- minute pre-incubation step at 37º C with gentle shaking, reactions were initiated by the addition of ADMA (100 µM). After 60 minutes, the incubation reactions were terminated and CIT extracted, reconstituted, and analysed as described in paragraph 3.2.5.3. The inhibitory potential of each compound was assessed over three independent experiments performed in singlicate. The concentration of CIT formed in each sample was calculated by comparing the peak area ratio CIT to IS for each sample to a CIT calibration curve in the concentration range 0 - 10 µM. Graphical representation of experimental data was obtained using GraphPad Prism (version 9.0 for Windows: GraphPad Software, San Diego, California USA).

3.3.6 Statistical analysis

Results are expressed as means ± standard deviation (SD) or standard error of the mean (SEM) as appropriate. Means, SD, SEM and %CV were determined using Excel (Microsoft Office 365 ProPlus, licenced to Flinders University).

Kinetic constants (K_m, V_{max}) for L-citrulline formation were derived from fitting the Michaelis-Menten equation below to experimental data using the nonlinear curve fitting software GraphPad Prism (version 9.0 for Windows: GraphPad Software, San Diego, California USA). Goodness of fit was assessed from the 95% confidence intervals, r^2 value, and standard error of the parameter fit.

$$Vo = \frac{V_{max}[S]}{Km + [S]}$$

V0 = Initial velocity (moles/times)
[S] = substrate concentration (molar)
V_{max}= maximum velocity
K_m = substrate concentration at half V_{max}

In inhibition experiments, one-way ANOVA was used to detect differences between groups and inhibition trend was considered as statistically significant for $p < 0.05$ (*), $p < 0.01$ (**), $p < 0.001$ (***) and $p<0.0001$ (****). One-way ANOVA with multiple comparisons was also performed to compare each inhibitor concentration to baseline (0 µM inhibitor) and inhibition was considered statistically significant for $p < 0.05$ (*), $p < 0.01$ (†), $p < 0.001$ (#) and $p<0.0001$ (^).

Chapter 4 - RESULTS

4.1 Colorimetric protein assays

Measuring protein concentration accurately is important to compare outcomes from one experiment to the next. In this project, varied methods were used to quantify unknown protein concentration, each of them with their own advantages and disadvantages, as described in Chapter 3. While the Lowry Protein assay failed to provide a valid linear standard curve, a good fit between experimental data and theoretical equation was obtained with both Bradford and EZQ assay. Bradford assay was chosen as the best method to measure the total protein concentration of *h*DDAH1-expressing HEK293T cell lysate due its being inexpensive, easy to perform, and providing consistent results across different days.

4.1.1 Lowry assay

The quantification of total protein concentration in the cell lysates, was firstly attempted by performing a Lowry assay. The assay was performed unsuccessfully multiple times and, as can be observed from the results reported in figure 6, the calibration curve was not linear, with a very low R-squared (R^2) value associated with the linear fit of the data ($R^2 = 0.8331$). Troubleshooting was attempted using different plate formats, freshly prepared batches of BSA and assay solutions and different equations to interpolate the experimental data, but with no improvement, thus the method was discarded, and different protein assays were evaluated (section 4.1.2).

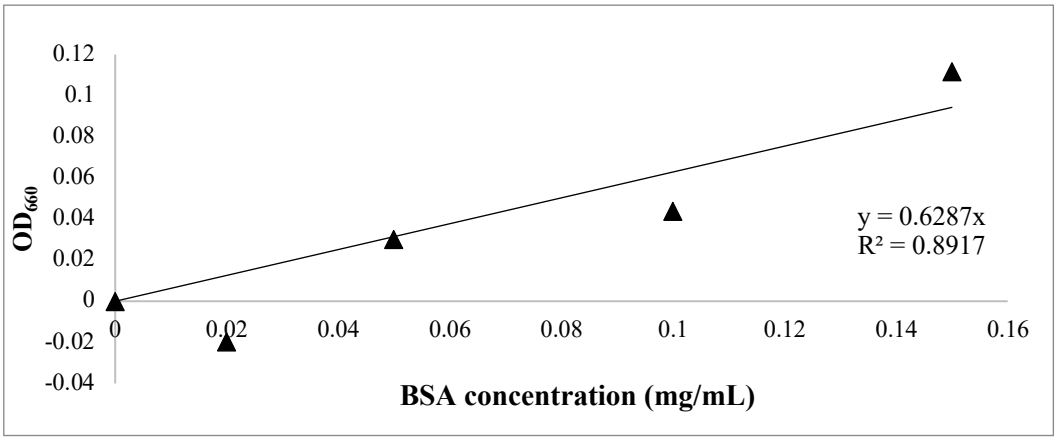

Figure 6: Representative of a Lowry protein assay, mean of the OD at 660 nm plotted *versus* protein concentration (mg/mL). BSA protein (0, 0.2, 0.05, 0.1 and 0.15 mg/mL) was used as the standard for the calibration curve. Data points are singlicate values. Graph and tendency line were obtained through Microsoft® Excel® for Microsoft 365 (version 2019).

4.1.2 Bradford assay

The quantification of the total protein concentration of the cell lysates was also determined by Bradford assay and the results are represented in table 3 and figures 7 and 8. The assay was performed on the same samples in triplicate in two different days and the concentrations determined were averaged and reported in table 3. Polynomial (quadratic) regression (Figure 7) provided a better interpolation of the experimental data ($R^2 = 0.9965$) compared to linear regression ($R^2 = 0.976$, Figure 8), thus the quadratic equation in figure 7 was used to calculate the unknown protein concentrations of the samples in table 3.

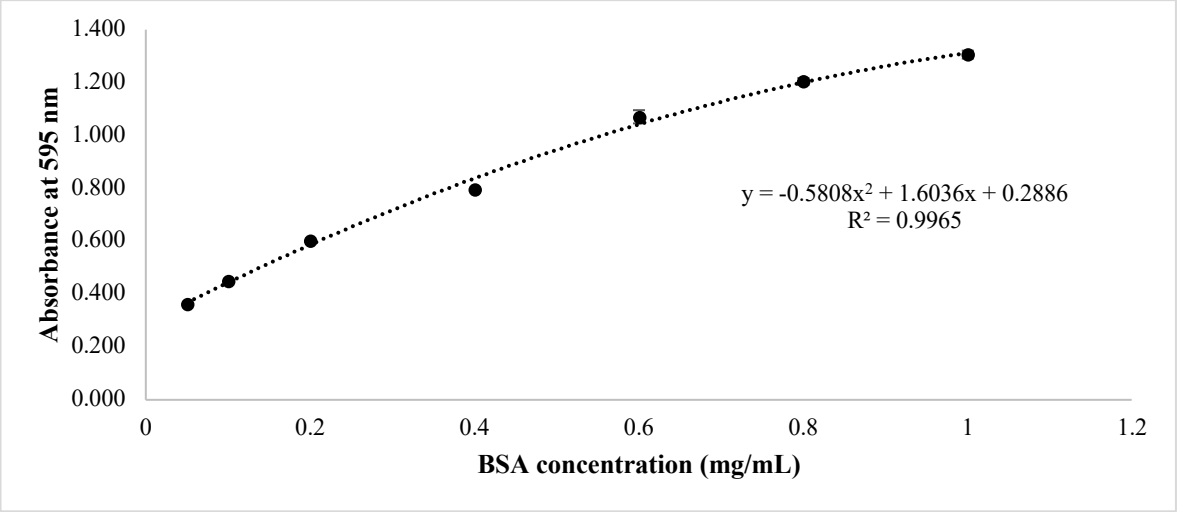

Figure 7: Representative of Bradford protein assay calibration data interpolated using quadratic regression, mean of the OD at 595 nm plotted *versus* protein concentration (mg/mL). BSA protein (0.05, 0.1, 0.2, 0.4, 0.6, 0.8, 1 mg/mL) was used as the standard for the calibration curve. Plotted data are the mean of three replicate measurements and error bars represent the STD. Graph and tendency line were obtained through Microsoft® Excel® for Microsoft 365 (version 2019).

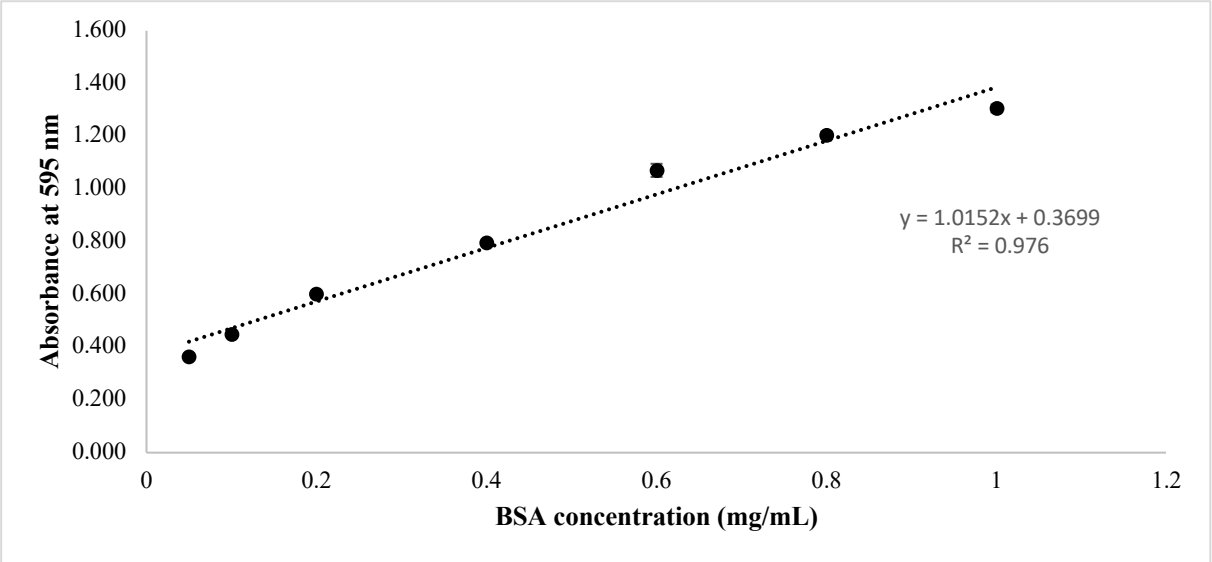

Figure 8: Representative of Bradford protein assay calibration data interpolated with the linear equation, mean of the OD at 595 nm plotted *versus* protein concentration (mg/mL). BSA protein (0.05, 0.1, 0.2, 0.4, 0.6, 0.8, 1 mg/mL) was used as the standard for the calibration curve. Plotted data are the mean of three replicate measurements and error bars represent the STD. Graph and tendency line were obtained through Microsoft® Excel® for Microsoft 365 (version 2019).

SAMPLE	Mean OD_{595}	[PROTEIN] ± STD - µg / µL
HEK 293T DDAH1 untransfected negative control lysate	0.57	3.55 ± 0.32
HEK 293T DDAH1 untagged positive control lysate	0.74	2.78 ± 0.54
HEK 293T FLAGDDAH2 negative control lysate	0.57	3.46 ± 0.35
HEK 293T FLAGDDAH1 positive control lysate	0.79	5.98 ± 0.97
HEK 293T DDAH1 untagged preparation 1	0.66	4.59 ± 0.66
HEK 293T DDAH1 untagged preparation 2	0.74	8.14 ± 0.74

Table 3: Determination of protein concentration by Bradford assay. Mean OD_{595}, and average protein concentration ± standard deviation are reported. Values are the mean of two independent experiments performed in triplicate.

Concentrations of positive (**HEK293T DDAH1 untagged positive control lysate**, concentration 2.78 mg/mL, and **HEK293T FLAGDDAH1 positive control lysate**, concentration 5.98 mg/mL) and negative controls (**HEK293T untransfected negative control lysate**, concentration 3.55 mg/mL, and **HEK293T FLAGDDAH2 negative control lysate**, concentration 3.46 mg/mL) reported in table 3 overall agreed with the values reported on the vial tubes, which are as follows:

- **HEK293T DDAH1 untagged positive control lysate** = 3.02 mg/mL
- **HEK293T FLAGDDAH1 positive control lysate** = 6.11 mg/mL
- **HEK293T FLAGDDAH2 negative control lysate** = 4.80 mg/mL
- **HEK293T untransfected negative control lysate** = 3.41 mg/mL

The lower concentration measured for **HEK293T FLAGDDAH2 negative control lysate** is likely the result of partial protein degradation following long term storage (more than 12 months) of the lysate at -20º C. **HEK293T DDAH1 untagged preparation 1** and **2** were both generated as part of this project and the second batch showed a higher protein

concentration (8.14 mg/mL) compared to the first batch (4.59 mg/mL), thus it was selected as the DDAH1 enzyme source for all the incubation experiments.

4.1.3 EZQ assay

EZQ assay was also used to determine the protein concentrations of the two batches of *h*DDAH1-expressing HEK293T cell lysate (**HEK293T DDAH1 untagged preparation 1** and **2**). Figure 9 represents the calibration curve obtained from the ovalbumin standards and shows again a good fit between experimental data and the quadratic equation ($R^2 = 0.999$). The values for total protein concentrations measured for the two preparations of HEK293T DDAH1 untagged lysates were 4.67 and 8.02 mg/mL, respectively and consistent with the protein concentrations of the same samples measured using the Bradford assay (4.59 and 8.14 mg/mL, respectively), thus confirming an accurate measurement of protein concentrations.

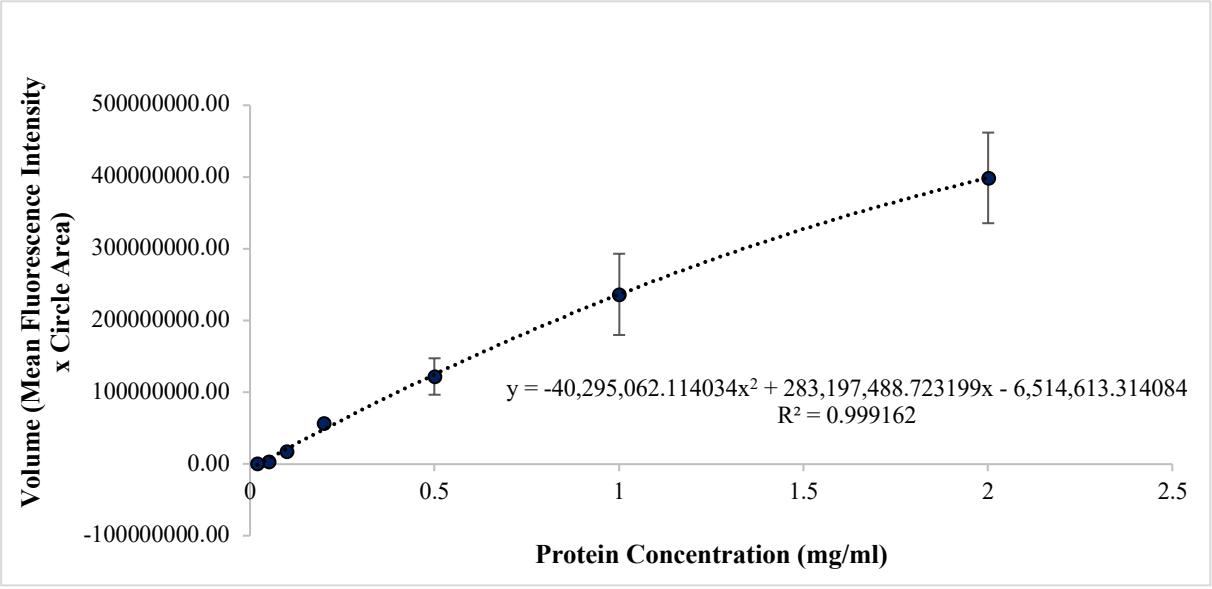

Figure 9: Representative of EZQ assay calibration curve. Data is interpolated using quadratic regression, mean volume, corresponding to the product between mean fluorescence intensity and circle area, is plotted versus protein concentration (mg/mL). The standard curve is generated from dilution series of ovalbumin standards (0.02, 0.05, 0.1, 0.2, 0.5, 1, 2 mg/mL). Plotted data are the mean of three replicate measurements and error bars represent the STD. Graph and tendency line were obtained through Microsoft® Excel® for Microsoft 365 (version 2019).

4.2 Expression of *h*DDAH1 lysate by Western Blot analysis

Western Blot was performed to detect the presence of the enzyme DDAH1 in the protein lysates and results are reported in figure 10.

A previously characterised DDAH1 and FLAGDDAH1-expressing HEK293T cell lysates were used as positive control (Tommasi, Sara et al. 2015) while untransfected HEK293T and FLAGDDAH2-expressing HEK293T cell lysates were used as negative control. According to the primary antibody manufacture (Abcam), DDAH1 produces a band at 37 kDa. Figure 10 – panel A shows the results of immunoblotting with anti-DDAH1 primary antibody. As expected, immuno-reactive bands were observed in lanes 3, 5, 6, and 7 corresponding to the two preparations of *h*DDAH1-expressing HEK293T cell lysate (lanes 6 and 7) and the two positive controls (lane 3 and 5). Contrarily, no band was detected in lanes 2 and 4 corresponding to negative controls. The DDAH1 band in lane 5 ran slightly higher than the other DDAH1 bands, due to presence of the FLAG-tag, a sequence of 8 amino acids (DYKDDDDK) commonly incorporated into fusion proteins to allow for isolation, purification, identification and immunoprecipitation of tagged proteins (Gerace & Moazed 2015). An additional band was observed in all lanes with an estimated molecular weight of 55 kDa and this was the result of non-specific binding of the antibody. Figure 10 – panel B shows the results of immunoblotting with mouse anti-FLAG primary antibody. As expected, immuno-reactive bands were observed in lane 5 at 37 kDa corresponding to FLAGDDAH1 and in lane 4 around 29 kDa corresponding to FLAGDDAH2. The same band previously observed in panels A is noticeable in all lanes at around 55 kDa, further confirming that said band is likely the result of non-specific fluorescence. In conclusion, western blotting demonstrated that the protein of interest, *h*DDAH1, was expressed in both batches of *h*DDAH1-expressing HEK293T cell lysate.

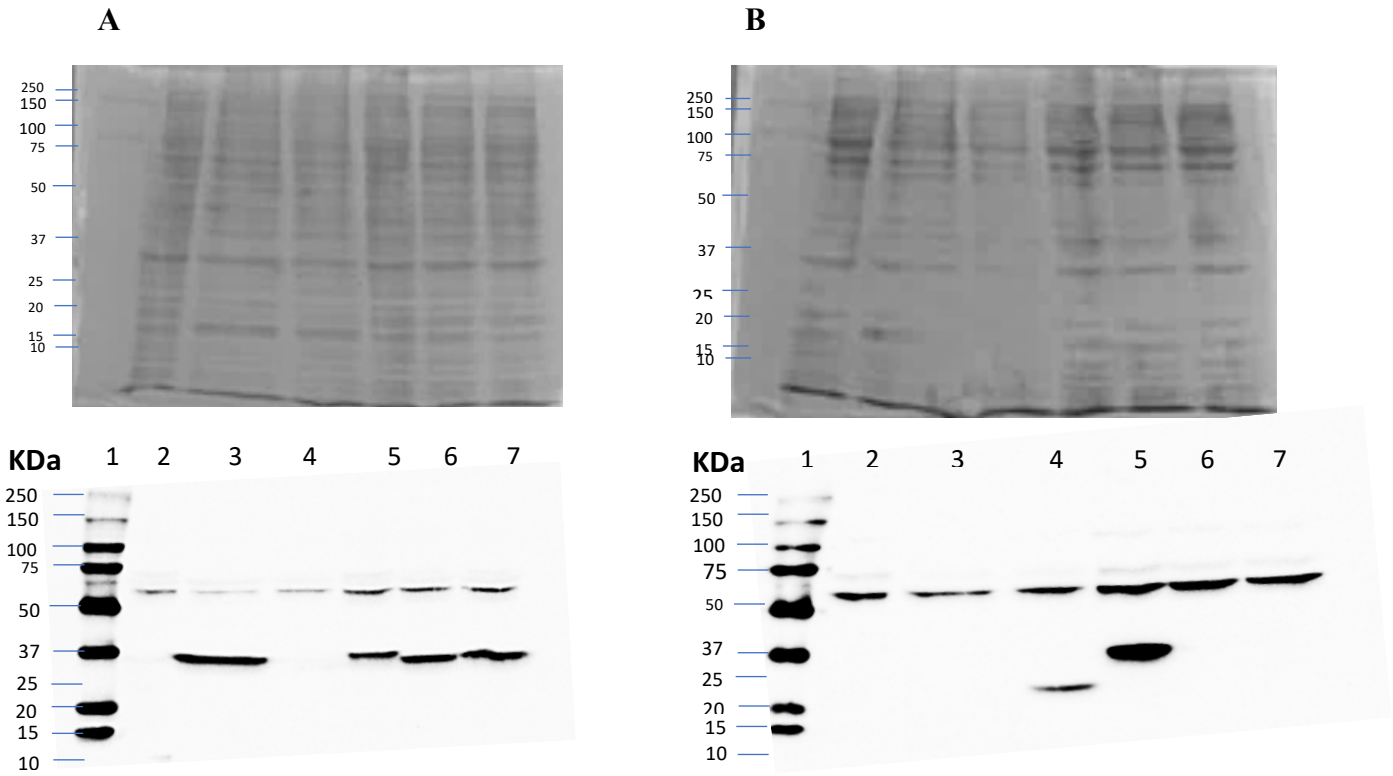

Figure 10: Detection of *h*DDAH1 expression by immunoblotting. HEK293T cell lysates (30 µg) were separated by SDS-PAGE on a 4-10% acrylamide gel, then transferred to a nitrocellulose membrane and probed with anti-DDAH1 primary antibody (panel A) and anti-FLAG primary antibody (panel B). For each panel, top image represents the polyacrylamide gel post transfer following staining with Coomassie brilliant blue, while the bottom image represents the probed nitrocellulose membrane. Each gel and blot contain: Molecular weight markers (MM; lane 1), untransfected HEK293T cell lysate (lane 2, negative control), untagged DDAH1 lysate (lane 3, positive control), FLAGDDAH2 cell lysate (lane 4, negative control), FLAGDDAH1 lysate (lane 5, positive control), untagged DDAH1 preparation 1 (lane 6) and untagged DDAH1 preparation 2 (lane 7). The immuno-reactive bands occurred at 37 kDa (panel A) and at both 37 and 29 kDa (panel B).

4.3 *h*DDAH1 activity assay

4.3.1 UPLC-MS analysis

During this project, the column and conditions of the UPLC-MS method were changed from what previously reported (Tommasi et al. 2017) due constant failure of said method, such as nonlinear calibration curves and elevated inter and intra-assay variability indicating that the integrity of the column was compromised. Due to significant delays in the delivery of a new column caused by the COVID-19 pandemic, a new method using a different column available

within the lab, was developed. Following assay validation, the enzymatic system was characterised in the absence of any inhibitor first and then the inhibitory potential of the different compounds was evaluated (section 4.4).

Representative chromatograms for CIT and the IS CIT–d6 are reported in Figure 11. Both CIT and CIT-d6 exhibited spontaneous fragmentation in the MS source and generated analyte specific fragments (176.10→159.14 for CIT and 181.13→165.17 for CIT-d6) that resulted in peaks with higher signal intensity than their corresponding molecular ions. Quantification using these fragments provided better sensitivity and was therefore used in this method. CIT was eluted at a retention time of 10.86 ± 0.06 min, while CIT-d6 was eluted at a retention time of 10.88 ± 0.06 min. Small changes in column and auto-sampler temperatures and the use of different solvent batches did not impact on retention time, peak areas and calibration curve slope, thus indicating that the method is robust.

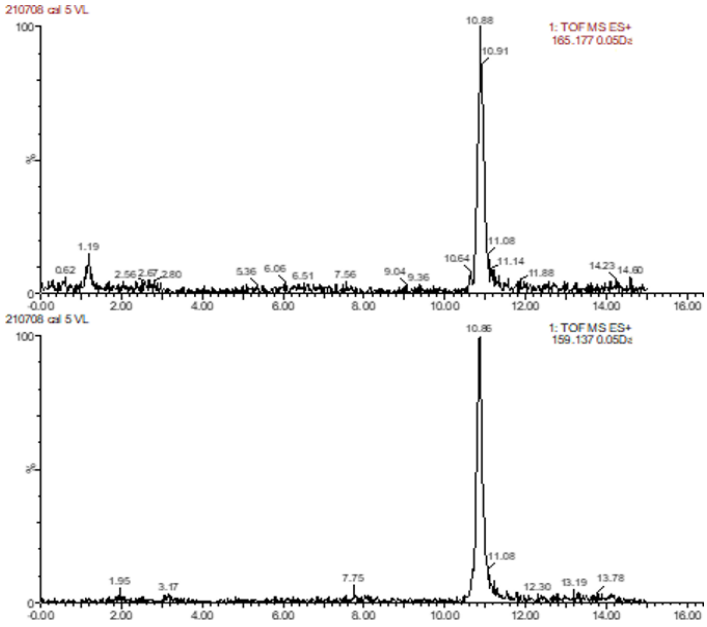

Figure 11: Representative chromatograms of CIT-d6 (IS, top) and CIT (bottom) for analyte quantification. Chromatograms were extracted using MassLynx (version 4.1, Waters Australia) at m/z of 165.17 and 159.14 corresponding to the specific fragments of CIT-d6 and CIT, respectively. Chromatograms are shown for calibrator 6 corresponding to a CIT concentration of 10 µM.

LLOD, the smallest amount or concentration of the analyte in the test sample that can be reliably distinguished from zero, was calculated as the CIT concentration corresponding to a signal-to-noise ratio of 2:1. LLOQ, the lowest concentration of the analyte that can be determined with an acceptable repeatability and trueness, was calculated as the CIT concentration corresponding to a signal-to-noise ratio of 5:1 (González & Alonso 2020). LLOD and LLOQ were 0.4 and 1 µM, respectively.

Method reproducibility was assessed *via* determination of the instrument and method precision (table 4) and of intra- and inter-day variability (tables 5 and 6).

Method precision

Instrument precision		**Method precision**	
sample	**peak area ratio**	**sample**	**peak area ratio**
replicate 1	0.668	replicate 1	0.660
replicate 2	0.679	replicate 2	0.517
replicate 3	0.696	replicate 3	0.669
replicate 4	0.674	replicate 4	0.727
replicate 5	0.683	replicate 5	0.678
replicate 6	0.692	replicate 6	0.670
		replicate 7	0.668
Average value	**0.682**	**Average value**	**0.656**
STD	**0.011**	**STD**	**0.065**
%CV	**1.5**	**%CV**	**9.9**

Table 4: Parameters of assay precision. In the instrument precision evaluation, each replicate corresponds to the repeated injection and peak area quantification of the same sample. In the method precision assessment, each replicate corresponds to the injection and peak area quantification of individual samples prepared at the same nominal CIT concentration of 8 µM.

Intra-day repeatability	
Nominal concentration (µM)	**8**
replicate 1	8.5
replicate 2	6.7
replicate 3	8.6
replicate 4	9.4
replicate 5	8.7
replicate 6	8.6
replicate 7	8.6
Average value	**8.4**
STD	**0.9**
%CV	**10.9**
Accuracy (%)	**105**

Table 5: Intra-day repeatability. Each replicate corresponds to the injection and CIT concentration quantification of individual samples prepared at the same nominal CIT concentration of 8 µM and measured within the same day.

Inter-day repeatability		
Nominal concentration (µM)		**8**
Day 1	replicate 1	8.5
	replicate 2	6.7
	replicate 3	8.6
	replicate 4	9.4
	replicate 5	8.7
	replicate 6	8.6
	replicate 7	8.6
Day 2	replicate 1	8.1
	replicate 2	8.1
Day 3	replicate 1	8.1
	replicate 2	8.0
Day 4	replicate 1	8.0
	replicate 2	7.9
Day 5	replicate 1	8.3
	replicate 2	8.1
Day 6	replicate 1	7.9
	replicate 2	8.2
Average value		**8.2**
STD		**0.6**
%CV		**6.8**
Accuracy (%)		**101**

Table 6: Inter-day repeatability. Each replicate corresponds to the injection and CIT concentration quantification of individual samples prepared at the same nominal CIT concentration of 8 µM and measured across 6 days.

High levels of instrument and method precision were observed with %CVs below 10% (1.5% and 9.9%, respectively) (table 4). The method was also highly repeatable within the same day with a %CV of 11% and good accuracy despite a small overestimation of CIT concentration (105% accuracy). Similarly, high precision and accuracy were obtained across 6 days (%CV = 6.8% and Accuracy = 101%).

4.3.1.1 Preparation of standards

Calibration curves were obtained by plotting the peak area ratio CIT to IS versus the concentration of CIT. All standard curves obtained with concentrations of L-CIT comprised between 0 and 10 µM showed a good linearity with R^2 values comprised between 0.9981 and 0.9999. A representative calibration curve is reported in figure 12.

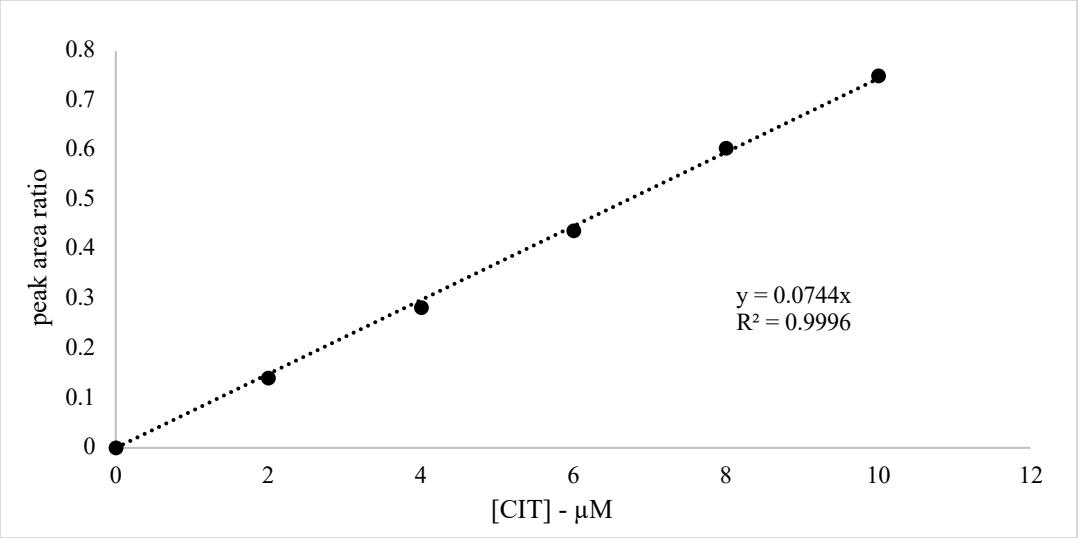

Figure 12: Representative of calibration curve. CIT standard concentrations are 0, 2, 4, 6, 8 and 10 µM. Peak area ratio CIT to IS is plotted against CIT concentration. Graph and tendency line were obtained through Microsoft® Excel® for Microsoft 365 (version 2019), points are experimentally determined values of singlicates measures, whereas lines are from model-fitting.

4.3.2 Protein and time linearity

In order to characterise the kinetic behaviour of DDAH1 (section 4.3.3), linear conversion of ADMA into CIT was assessed under different incubation conditions. Figure 13 – panel A

shows the effect of varying the enzyme concentration in the incubation mixture; a linear increase in CIT concentration is observed in relation to total protein. CIT formation was evaluated at different protein concentrations (0, 0.25, 0.5, 0.75, 1 mg/mL), while maintaining constant ADMA concentrations and incubation time. A linear relationship was observed between the concentration of CIT formed and total protein when mixtures incubated for 50 min in the presence of either 50 or 500 µM ADMA ($R^2 = 0.9993$ and $R^2 = 0.9999$, respectively). In addition, time linearity was also determined at different incubation times (0, 20, 40, 60, 80 min), while protein concentration and substrate (ADMA) were kept constant. A linear relationship was again observed between the concentration of CIT formed and the incubation time for mixtures containing a constant enzyme concentration (total protein = 0.5 mg/mL) and either 50 or 500 µM ADMA ($R^2 = 0.9994$ and $R^2 = 0.9997$, respectively, Figure 13– panel B). Based on these data, a linear conversion of ADMA to CIT was observed up to 1 mg/mL of total protein and 80 min of incubation time, thus the experimental conditions for all the following experiments were maintained within these ranges and adjusted based on specific needs for signal intensity, while minimizing waste of time and materials.

4.3.3 Characterization of the kinetic behaviour of the *h*DDAH1 expression system

Further kinetic investigation of the ADMA metabolism by *h*DDAH1 containing cell lysate was performed according to the method described in section 3.3.4.6. The conversion of ADMA to CIT was characterised in three independent experiments at *h*DDAH1-expressing HEK293T cell lysate total protein concentration of 0.5 mg/mL and incubation time of 60 min. A hyperbolic relationship was observed between the rate of CIT formation and ADMA concentrations (Figure 13 – panel C) and the Michaelis-Menten equation best modelled the experimental data. The kinetic parameters K_m and V_{max} estimated using the Eadie – Hoffstee transform (124.6 µM and 869.3 pmol*mg^{-1}*min^{-1}, respectively, Figure 13 – panel D) were in

agreement with those derived from non-linear least squares fitting of experimental data using GraphPad Prism software (version 9.0), K_m = 111.9 ± 9.1 µM and V_{max} = 839.1 ± 23.3 pmol*mg^{-1}*min^{-1} (table 7).

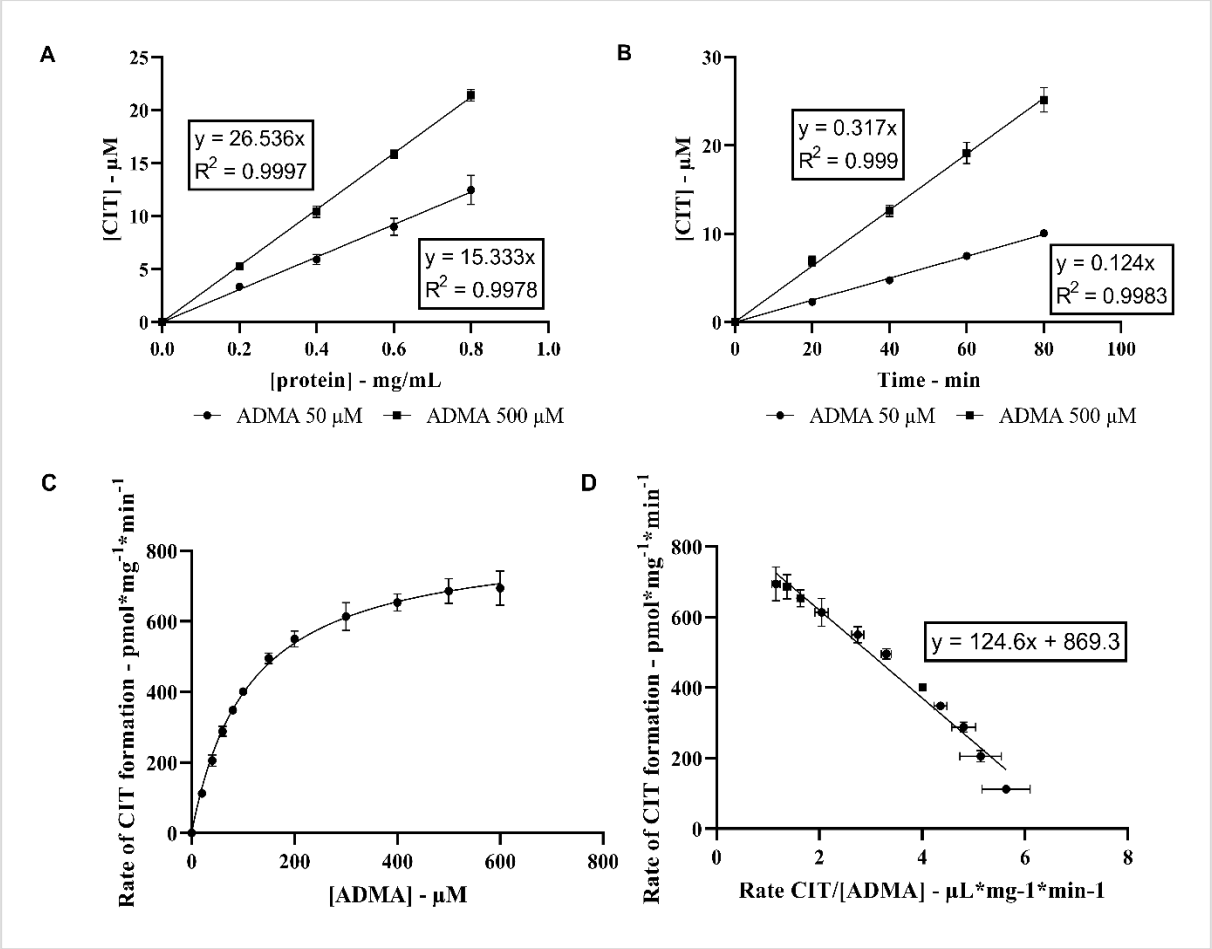

Figure 13: The kinetic plots representing the conversion of ADMA to L-CIT by *h*DDAH1. Protein (A) and time (B) linearity data are shown at ADMA concentration of 50 µM and 500 µM. ADMA concentration is plotted *versus* rate of CIT formation (C). The data is represented as the Michaelis-Menten fit (panel C) and its Eadie-Hoffstee transform (R^2 value of 0.8962 is not reported on the plot) (D). Each data point represents the mean of three singlicate experiments, and error bars represent the SEM. Graph and tendency line were obtained through GraphPad Prism (version 9.0 for Windows).

Parameter	Replicate 1	Replicate 2	Replicate 3	Mean
K_m (μM) ± SEM	123.4	105.9	106.1	111.9 ± 9.1
95% confidence interval K_m	112.3-135.5	89.43-125.2	92.37-121.9	93.35-130.4
V_{max} (pmol*min^{-1}*mg^{-1}) ± SEM	944.9	784.3	789.0	839.1 ± 23.3
95% confidence interval V_{max}	916.3-979.3	741.9-830.8	753.5-827.3	791.9-886.4
R-squared	0.998	0.9932	0.9953	0.9753

Table 7: Kinetic parameters for the conversion of ADMA to CIT by *h*DDAH1. Values are derived from fitting the Michaelis-Menten equation to three singlicate experimental data and to the average of the three experiments using the nonlinear curve fitting function in GraphPad Prism (version 9.0 for Windows).

An ADMA concentration of 100 μM was chosen for the inhibition studies since this value is close to the enzyme K_m, thus it is located in an area of the Michaelis-Menten curve in which small changes in ADMA concentrations are associated with larger changes in CIT formation.

4.4 Screening of potential novel *h*DDAH1 inhibitors

After establishing the best incubation parameters (incubation time, protein, and ADMA concentration) based on the described experiments, six molecules identified by AI and one compound designed within Clinical Pharmacology lab were screened based on their potential to inhibit *h*DDAH1. A broad range of five concentrations of each inhibitor (0, 0.1, 1, 10, 100 μM) was selected for these experiments and the results are represented in figure 14 (panels A and B). ZST316 (compound 10a) (Murphy et al. 2016; Tommasi, Sara et al. 2015) was used as a positive control (Figure 14 – panel A, pink bars and red arrows) for *h*DDAH1 inhibition at the concentrations of 0.1 and 1 μM**.** These values were chosen based on its reported K_i of 1 μM. According to the data collected, none of the screened compounds that were designed by AI reached significant inhibition of *h*DDAH1 activity in the range of concentrations studied (0 – 100 μM). Higher concentrations were not investigated, as the aim was to identify novel inhibitors with either $K_i < 10$ μM or $IC_{50} < 20$ μM. Compound ZIR26 (Figure 14 – panel A dark

blue bars and purple arrows) designed within the Clinical Pharmacology lab was the only molecule in this series to exhibit a significant inhibition potency ($p < 0.0001$, Figure 14 – panel B), albeit less potent than the reference compound ZST316 (36% inhibition at 1 μM *versus* 62% inhibition obtained with ZST316). Based on data represented in figure 14, the IC_{50} for ZIR26 lies between 1 and 10 μM, thus confirming the hypothesis that at least one of the 7 compounds investigated would have showed good *h*DDAH1 inhibitory potential. More detailed characterisation of the kinetics of *h*DDAH1 inhibition to allow a more precise derivation of IC_{50} and K_i values is warranted but was not performed due to time constraints.

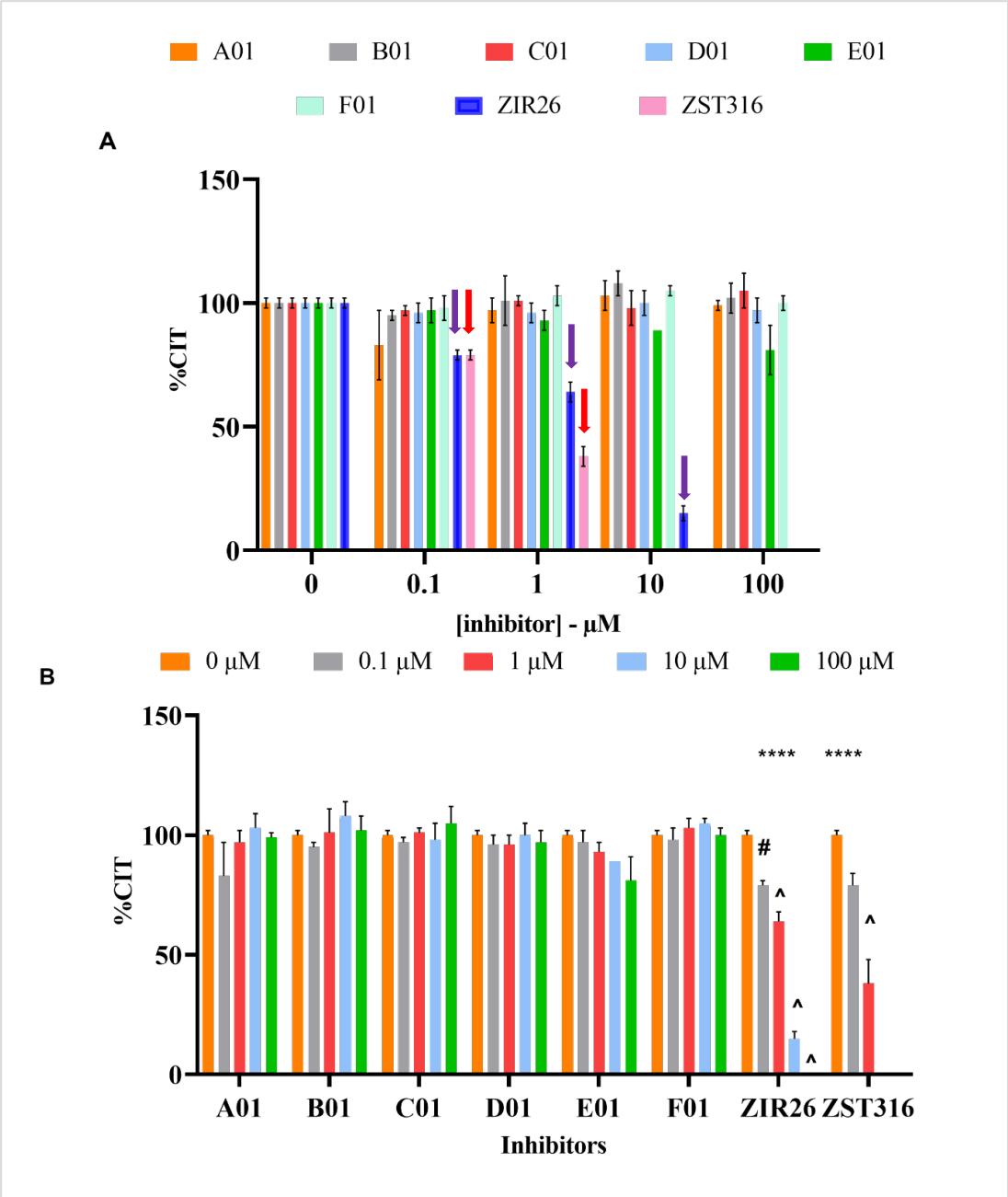

Figure 14: Screening of the inhibitory activity of 7 compounds on *h*DDAH1. ZST316 used as a positive control and indicated by a red arrow. (A) On the x-axis, the concentration of each potential inhibitor is reported in µM, and on the y-axis the percentage of CIT formation relative to control (0 µM) expresses the enzyme activity. (B) On the x-axis is reported each potential inhibitor and on the y-axis the percentage of CIT formation relative to control (0 µM) expresses the enzyme activity. Each data point represents the mean of three independent experiment performed in singlicate. Error bars indicate the SEM. Graphs were obtained through GraphPad Prism (version 9.0 for Windows), ****$P < 0.0001$ for trend; #$P < 0.001$ vs. baseline; ^$P < 0.0001$ vs. baseline.

Chapter 5 – DISCUSSION

Current literature suggests that the development of novel *h*DDAH1 inhibitors might lead to the introduction of a novel class of pharmacological agents in clinical practice. By targeting the NO/ADMA/DDAH pathway these novel therapeutics have the potential to treat diseases caused by excessive NO. Recent studies have reported that *h*DDAH1 inhibition could represent a novel therapeutic approach for the treatment of many diseases, such as septic shock (Wang et al. 2014), prostate (Kami Reddy et al. 2019), triple negative breast cancer (Hulin et al. 2019) and pulmonary fibrosis (Pullamsetti et al. 2011). Furthermore, the compounds might also be used to investigate the importance of DDAH in other species. Despite the fact that this novel therapeutic strategy is being studied by many research groups, only a small number of *h*DDAH1 inhibitors with similar chemical structure have been examined *in vivo* and there is large scope for the development and the investigation of novel compounds with diversified chemical structures and improved pharmacokinetic profiles.

In this study, the inhibition activity of seven novel potential *h*DDAH1 inhibitors has been reported using a robust UPLC-MS based *h*DDAH1 activity assay to measure the efficiency of HEK293T cell lysates overexpressing recombinant *h*DDAH1 to catalyse the conversion of ADMA into CIT. A new DDAH1 activity assay was developed because the previously published method (Tommasi et al. 2017) could not be applied since the UPLC column was underperforming. Due to the extenuating circumstances related to the COVID-19 pandemic, the replacement of a faulty column was not achievable in a time range compatible with the current project, so the method for CIT detection was re-developed and validated using different column and analytical conditions, according to the methodology outlined in Chapter 3. Similarly to what previously reported (Tommasi et al. 2015, Tommasi et al. 2017), the current method used *h*DDAH1 overexpressing HEK293T cell lysate as the source of *h*DDAH1 enzyme.

The choice of using cell lysate instead of the purified protein allowed to avoid the risk of compromising the structural and functional integrity of the enzyme during the purification process, to reduce costs and to perform the experiments using conditions that are closer to the physiological environment since the lysate carries all the biomolecules and ions normally present in the cell cytosol (Tommasi et al. 2017). The total protein content of the freshly prepared lysates was quantified using the Bradford protein assay and the accuracy of the measurement confirmed by EZQ assay. Furthermore, qualitative Western blot analysis confirmed that *h*DDAH1 was highly expressed in the lysates as demonstrated by the high intensity of the bands obtained with merely 30 µg of total protein.

The analytical conditions used in this project exhibit important differences from what previously reported by the Department of Clinical Pharmacology (Tommasi et al. 2015, Tommasi et al. 2017), which resulted in the new method being less sensitive than the one previously developed (LLOD = 0.4 *versus* 0.1 µM and LLOQ = 1 µM *versus* 0.2 µM). Another difference from the previous method consists in the length of the chromatographic run. The current method requires a 15-minute run, much longer than the 8-minute of the method in Tommasi et al. (2015), with the obvious limitation that measurements are more time consuming and require a larger volume of solvents. The increased length of each run might also represent a limitation in terms of increasing the risk of degradation of the samples, but this was not an issue in this project, as demonstrated by the fact that repeated measurements of the same calibrators at the beginning and the end of each run gave consistent results (data not shown), which also demonstrated a consistent instrument performance throughout each individual experiment. Nevertheless, the newly developed method demonstrated to be robust and highly accurate and precise (both intra- and inter-day %CV less than 11% and accuracy = 105%) according to the standards reported by the Bioanalytical Method Validation Guidance for Industry issued by the FDA (FDA, 2018) that indicate that %CV should be in the range of ±

15-20% and accuracy should be close to 100% with a margin of ± 20%. Furthermore, the level of sensitivity achieved was sufficient for its application in the inhibition experiments herby reported. Further experiments are warranted to ameliorate the method validation, particularly determination of precision, accuracy and repeatability at additional CIT concentrations including LLOQ.

The characterisation of the enzymatic system in the absence of any inhibitor allowed the determination of the kinetic parameters K_m and V_{max} that corresponded to 111.9 μM and 839.1 pmol*mg^{-1}*min^{-1}, respectively. Despite the low R^2 value of the Eadie-Hoffstee plot (R^2 = 0.8962), likely caused by insufficient instrument sensitivity and incapability to measure the lowest concentrations of CIT accurately, non-linear least squares fitting of experimental data identified the Michaelis-Menten equation as the best model to describe *h*DDAH1 behaviour. The K_m value agrees with what previously reported by our research group in 2015, K_m = 103 μM (Tommasi et al. 2015), using a similar system. Higher variability was observed with V_{max} (V_{max} = 839.1 *versus* V_{max} = 258 pmol*mg^{-1}*min^{-1} (Tommasi et al. 2015), V_{max} = 353 pmol*mg^{-1}*min^{-1} (Tommasi et al. 2017), V_{max} = 356 pmol*mg^{-1}*min^{-1} (Forbes et al. 2008)), but this was expected since K_m is a constant value specific to the enzyme, while V_{max} tends to vary across different batches. The discrepancy can be explained with the fact that different batches of cell lysate can have a different proportion of *h*DDAH1 enzyme relative to total protein, nevertheless the values of V_{max} reported in this work are significantly higher than those previously reported and additional replicates of the experiment are required to investigate this difference. Techniques are available to quantify the *h*DDAH1 content in cell lysate, such as quantitative western blot and proteomics, however the former was previously attempted within our lab and failed to provide accurate and reliable quantification of *h*DDAH1, while the latter is a highly expensive technology. The exact *h*DDAH1 content quantification was not deemed necessary for the scope of this project, since all inhibition experiments were performed using the same

batch of lysate and a constant total protein concebtration. Other studies (Forbes et al. 2008) have reported lower values of K_m for recombinant *h*DDAH1 and its substrate ADMA and the difference is likely related to the use of purified His6-tagged recombinant *h*DDAH1 in these experiments. The introduction of the His6-tag and the process of purification might have caused small structural alteration to the enzyme and the loss of important cellular components (e.g., ions, other biomolecules) that might modulate the enzyme activity, thus changing its kinetic behaviour.

Since the difficulty in quantifying the exact *h*DDAH1 content in the protein source can lead to some variability, it is important to perform a detailed kinetic characterisation of any new lysate batch in the absence of any inhibitor and we chose to conduct all the kinetic experiments in this project using a single batch of cell lysate. All compounds studied were screened *in vitro* with the known *h*DDAH1 inhibitor ZST316 (positive control) under strict linear conditions *in vitro* using an incubation time of 60 minutes and protein concentration of 0.5 mg/mL (both within the limits of 80 minutes and 1 mg/mL determined with the time and protein linearity experiments), and at ADMA concentration of 100 µM, close to K_m. These values provided a good signal intensity allowing an accurate measurement of the capacity of each potential inhibitor to interfere with the rate of CIT formation in incubation reactions in which the enzyme and substrate concentration and incubation time were maintained constant. Interestingly, the herby reported method showed linear formation of CIT at higher protein concentrations that the one published by Tommasi et al. in 2017, which exhibited linearity up to 0.6 mg/mL (Tommasi et al. 2017).

Out of all the potential inhibitors investigated, compound ZIR26 was the only molecule to achieve significant inhibition at concentrations of 0.1, 1, 10 and 100 µM as shown in Figure 14 and the concentration of CIT formed in the presence of 100 µM of this inhibitor was below the LLOQ. Due to time constraint, a detailed characterisation of the kinetics of inhibition with

derivation of the kinetic parameters IC_{50} and K_i could not be performed, however this molecule was synthesised as an analogue of ZST316, so we can hypothesise that it will also exhibit competitive inhibition of *h*DDAH1 and the IC_{50} can be estimated to be comprised between 1 and 10 μM based on the data in Figure 14. The newly identified inhibitor is less effective than the positive control ZST316, K_i = 1 μM; IC_{50} = 3 μM (Tommasi et al. 2015), but further investigation is required to evaluate if improved pharmacokinetics properties can counterbalance its reduced inhibition potency. Nevertheless, based on the data discussed, the IC_{50} value for ZIR26 estimated between 1 and 10 μM confirms the hypothesis that at least one of the 7 compounds investigated would act as a *h*DDAH1 inhibitor with a $IC_{50} < 20$ μM.

On the contrary, none of the compounds designed by AI acted as a *h*DDAH1 inhibitor. The lack of any inhibitory effect with the 6 compounds investigated is not sufficient to establish if the AI algorithm have failed in identifying novel *h*DDAH1 inhibitors because of the blinded nature of the study. Due to the timeframe of the project, only 6 out of the 70 compounds provided Atomwise were investigated and these molecules could not be chosen based on their best ranking but needed to be randomly selected because of the conditions in the intellectual property agreement between the Department of Clinical Pharmacology and Atomwise. Furthermore, this agreement clearly specifies that negative controls were included in the group of compounds provided to our research group and all the compounds investigated in this study might have belonged to the negative control category. Over 6 rounds of the AIMS Awards Program, Atomwise has selected over 775 drug discovery projects and identified compounds to address over 600 targets (Atomwise, 2021). Only the screening of all the remaining molecules will give a true indication if changes in the algorithm (ideally guided by these experimental data) are required to optimise the identification of novel *h*DDAH1 inhibitors by AI.

5.1 Future perspectives

The next step from the proposed project would be to complete the screening of the remaining 64 compounds identified by AI. This could lead to the discovery of novel potent *h*DDAH1 inhibitors or highlight the need for Atomwise to reassess the parameters used to identify the 70 compounds in order to optimise the selection process. Furthermore, more libraries could be screened to identify new leads, and more compounds might be selected for *in vitro* screening.

ZIR26 has emerged in this study as a promising novel *h*DDAH1 inhibitor, but further characterisation of its inhibitory profile is required through the investigation of the mode of inhibition (irreversible *versus* reversible and in case of reversible inhibition it needs to be established if the compound works as a competitive, non-competitive, acompetitive or mixed inhibitor) and the accurate determination of *K*i and IC_{50} values. More specifically, an inhibition experiment using at least 10 inhibitor concentrations comprised between 1 and 10 µM would allow for a more accurate determination of the inhibitor IC_{50}, and *K*i could be determined in inhibition experiments using different concentrations of ADMA and inhibitors.

Furthermore, cell membrane permeability studies and a full pharmacokinetic characterisation of this compound are required to determine if ZIR26 has better chances of being developed into a pharmacological agent compared to the existing *h*DDAH1 inhibitors. Following these experiments, ZIR26 could then be used to study methylarginine-mediated NO regulation in a therapeutic context. ZIR26 induced *h*DDAH1 inhibition could be investigated in *in vitro* and *in vivo* models of pathological conditions associated with excessive NO production, such as aberrant neovascularisation and *vasculogenic mimicry* in TNBC (Hulin et al. 2019). Expertise and cellular models are available within our group to investigate the potential of compounds to inhibit tumour neovascularisation in TNBC cell lines (MDA-MB-

231 and BT549) and different assays could be performed to investigate if ZIR26 is able to inhibit the formation of vessel-like structures (Matrigel assay), cell proliferation and viability (crystal violet and MTT assays) and/or cell migration (scratch wound migration assay). ZIR26 could be investigated in other cellular models of cancers associated with excessive NO synthesis, such as LNCaP and PC3 (prostate cancer) and A375 (melanoma) and the effects of DDAH1 inhibition by ZIR26 on the expression of pro-angiogenic factors, such as VEGF, Hypoxia-inducible factor 1-alpha and the basic fibroblast growth factor.

SAR studies could also be performed to determine if structural modifications of ZIR26 would allow the improvement of its inhibition potency and/or pharmacokinetic properties. ZIR26 is structurally similar to ZST316, but with an ethyl substituent at the acylsulfonamidic function instead of a methyl group. Several substituents with different chemical and steric behaviour could be investigated at this position generating a library of second-generation DDAH1 inhibitors and ZST316 and ZIR26 analogues. Furthermore, the interaction between ZIR26 and the *h*DDAH1 active site could be investigated through site directed mutagenesis experiments.

More generically, a deeper understanding of the biological implications associated with changes in methylarginine concentrations and the development of specific therapeutic agents and strategies to reduce NO concentrations, is still a future objective that requires further investigation.

Thanks to the fact that DDAH1 is a highly conserved hydrolytic enzyme, its inhibition could also be explored in different species to gain better understanding of all the potential functions of this important enzyme.

5.2 Conclusion

In this work, a novel and robust UPLC-MS based assay was developed to measure the activity of recombinant human DDAH1 overexpressed in HEK293T cells. This constitutes a powerful instrument to determine the potential of novel compounds to inhibit the *h*DDAH1 catalysed conversion of ADMA into L-CIT. According to the *in vitro* data collected in this study, ZIR26 has revealed to be a potent *h*DDAH1 inhibitor and could be an ideal candidate to investigate the inhibition of excessive NO production in different *in vitro* and *in vivo* models of diseases.

REFERENCES

Alderton, WK, Angell, ADR, Craig, C, Dawson, J, Garvey, E, Moncada, S, Monkhouse, J, Rees, D, Russell, LJ, Russell, RJ, Schwartz, S, Waslidge, N & Knowles, RG 2005, 'GW274150 and GW273629 are potent and highly selective inhibitors of inducible nitric oxide synthase in vitro and in vivo', *British Journal of Pharmacology*, vol. 145, no. 3, pp. 301-12.

Aminian, M, Nabatchian, F, Vaisi-Raygani, A & Torabi, M 2013, 'Mechanism of Coomassie Brilliant Blue G-250 binding to cetyltrimethylammonium bromide: an interference with the Bradford assay', *Anal Biochem*, vol. 434, no. 2, pp. 287-91.

Arora D, Jain P, Singh N, Kaur H, Bhatla SC. 2016 'Mechanisms of nitric oxide crosstalk with reactive oxygen species scavenging enzymes during abiotic stress tolerance in plants.' *Free Radic Res.*; vol. 50, no. 3, pp. 291-303.

Atomwise Incorporated 2021, viewed 15 March 2021 <https://www.Atomwise.com/>.

Bailey, A, Pope, TW, Moore, SA & Campbell, CL 2007, 'The Tragedy of TRIUMPH for Nitric Oxide Synthesis Inhibition in Cardiogenic Shock', *American Journal of Cardiovascular Drugs*, vol. 7, no. 5, pp. 337-45.

Bioanalytical Method Validation Guidance for Industry 2018, viewed May 2018, < https://www.fda.gov/files/drugs/published/Bioanalytical-Method-Validation-Guidance-for-Industry.pdf/>

Bradford, MM 1976, 'A rapid and sensitive method for the quantitation of microgram quantities of protein utilizing the principle of protein-dye binding', *Analytical Biochemistry*, vol. 72, no. 1, pp. 248-54.

Brindicci, C, Ito, K, Torre, O, Barnes, PJ & Kharitonov, SA 2009, 'Effects of Aminoguanidine, an Inhibitor of Inducible Nitric Oxide Synthase, on Nitric Oxide Production and Its Metabolites in Healthy Control Subjects, Healthy Smokers, and COPD Patients', *Chest*, vol. 135, no. 2, pp. 353-67.

Carpenter, KA & Huang, X 2018, 'Machine Learning-based Virtual Screening and Its Applications to Alzheimer's Drug Discovery: A Review', *Current pharmaceutical design*, vol. 24, no. 28, pp. 3347-58.

Chan, HCS, Shan, H, Dahoun, T, Vogel, H & Yuan, S 2019, 'Advancing Drug Discovery via Artificial Intelligence', *Trends in Pharmacological Sciences*, vol. 40, no. 8, pp. 592-604.

Chung BH, Choi SK, Chang KC. 1996 'Effects of nitric oxide on detrusor relaxation.' *J Urol*., vol. 155, no. 6, pp. 2090-3.

Colasanti, M & Suzuki, H 2000, 'The dual personality of NO', *Trends in Pharmacological Sciences*, vol. 21, no. 7, pp. 249-52.

Cooke, JP 2003, 'NO and angiogenesis', *Atherosclerosis Supplements*, vol. 4, no. 4, pp. 53-60.

Cooke, JP, Losordo, DW. 2002 'Nitric oxide and angiogenesis.' *Circulation*. vol. 105, no. 18, pp. 2133-5.

Corbett, JA & McDaniel, ML 1996, 'The Use of Aminoguanidine, a Selective iNOS Inhibitor, to Evaluate the Role of Nitric Oxide in the Development of Autoimmune Diabetes', *Methods*, vol. 10, no. 1, pp. 21-30.

De Angelis Lobo d'Avila K, Gadonski G, Fang J, Dall'Ago P, Albuquerque VL, Peixoto LR, Fernandes TG & Irigoyen MC. 1999 'Exercise reverses peripheral insulin resistance in trained L-NAME-hypertensive rats.' *Hypertension* vol 34, pp. 768–772.

Dimmeler S, Hermann C, Galle J, et al. 1999 'Upregulation of superoxide dismutase and nitric oxide synthase mediates the apoptosis-suppressive effects of shear stress on endothelial cells.' *Arterioscler Thromb Vasc Biol.*, vol. 19, pp. 656–664.

Dulak J, Jozkowicz A, Dembinska-Kiec A, et al. 2000 'Nitric oxide induces the synthesis of vascular endothelial growth factor by rat vascular smooth muscle cells.' *Arterioscler Thromb Vasc Biol.* vol. 20, pp. 659–666.

Dumont, J, Euwart, D, Mei, B, Estes, S & Kshirsagar, R 2016, 'Human cell lines for biopharmaceutical manufacturing: history, status, and future perspectives', *Critical Reviews in Biotechnology*, vol. 36, no. 6, pp. 1110-22.

Esplugues JV. 2002 'NO as a signalling molecule in the nervous system.' *Br J Pharmacol.*vol.135, no. 5, pp. 1079-1095.
Fiedler, LR, Bachetti, T, Leiper, J, Zachary, I, Chen, L, Renné, T, Wojciak-Stothard, B. 2009 'The ADMA/DDAH pathway regulates VEGF-mediated angiogenesis.' *Arterioscler Thromb Vasc Biol*. vol. 2, no.12, pp. 2117-24.

Forbes, SP, Druhan, LJ, Guzman, JE, Parinandi, N, Zhang, L, Green-Church, KB & Cardounel, AJ 2008, 'Mechanism of 4-HNE Mediated Inhibition of hDDAH-1: Implications in No Regulation', *Biochemistry*, vol. 47, no. 6, pp. 1819-26.

Frey, D, Braun, O, Briand, C, Vasák, M & Grütter, MG 2006, 'Structure of the mammalian NOS regulator dimethylarginine dimethylaminohydrolase: A basis for the design of specific inhibitors', *Structure*, vol. 14, no. 5, pp. 901-11.

Fritsche, E, Bergner, A, Humm, A, Piepersberg, W & Huber, R 1998, 'Crystal Structure of l-Arginine:Inosamine-Phosphate Amidinotransferase StrB1 from Streptomyces griseus: An Enzyme Involved in Streptomycin Biosynthesis', *Biochemistry*, vol. 37, no. 51, pp. 17664-72.

Fulton, MD, Brown, T & Zheng, YG 2019, 'The Biological Axis of Protein Arginine Methylation and Asymmetric Dimethylarginine', *International Journal of Molecular Sciences*, vol. 20, no. 13.

Galkin, A, Kulakova, L, Demirkan, E, Lim, K, Howard, A & Herzberg, O 2004, *Structural Insight into Arginine Degradation by Arginine Deiminase, an Antibacterial and Parasite Drug Target**.

Gerace, E & Moazed, D 2015, 'Chapter Seven - Affinity Pull-Down of Proteins Using Anti-FLAG M2 Agarose Beads', in JR Lorsch (ed.), *Methods in Enzymology*, Academic Press, vol. 559, pp. 99-110.

Ghebremariam, YT, Erlanson, DA, Cooke, JP. 2014 'A novel and potent inhibitor of dimethylarginine dimethylaminohydrolase: a modulator of cardiovascular nitric oxide.' *J Pharmacol Exp Ther* vol. 348, no. 1, pp. 69-76.

Gillett, GT, McConville, CM, Byrd, PJ, Stankovic, T, Taylor, AM, Hunt, DM, West, LF, Fox, MF, Povey, S & Benham, FJ 1993, 'Irradiation Hybrids for Human Chromosome 11: Characterization and Use for Generating Region-Specific Markers in 11q14-q23', *Genomics*, vol. 15, no. 2, pp. 332-41.

González, O & Alonso, RM 2020, 'Validation of bioanalytical chromatographic methods for the quantification of drugs in biological fluids', in vol. 7, pp. 115-34.

Granados-Principal, S, Liu, Y, Guevara, ML, Blanco, E, Choi, DS, Qian, W, Patel, T, Rodriguez, AA, Cusimano, J, Weiss, HL, Zhao, H, Landis, MD, Dave, B, Gross, SS & Chang, JC 2015, 'Inhibition of iNOS as a novel effective targeted therapy against triple-negative breast cancer', *Breast Cancer Research*, vol. 17, no. 1, p. 25.

Gupta, R, Srivastava, D, Sahu, M, Tiwari, S, Ambasta, RK & Kumar, P 2021, 'Artificial intelligence to deep learning: machine intelligence approach for drug discovery', *Mol Divers*, vol. 25, no. 3, pp. 1315-60.

Habib, S & Ali, A 2011, 'Biochemistry of nitric oxide', *Indian journal of clinical biochemistry : IJCB*, vol. 26, no. 1, pp. 3-17.

Hafez, HM, Ibrahim, MA, Ibrahim, SA, Amin, EF, Goma, W & Abdelrahman, AM 2015, 'Potential protective effect of etanercept and aminoguanidine in methotrexate-induced hepatotoxicity and nephrotoxicity in rats', *Eur J Pharmacol*, vol. 768, pp. 1-12.

Hanafy, KA, Krumenacker, JS & Murad, F 2001, 'NO, nitrotyrosine, and cyclic GMP in signal transduction', *Med Sci Monit*, vol. 7, no. 4, pp. 801-19.

Hoffmann, J & Goadsby, PJ 2012, 'New Agents for Acute Treatment of Migraine: CGRP Receptor Antagonists, iNOS Inhibitors', *Curr Treat Options Neurol*, vol. 14, no. 1, pp. 50-9.

Hong, L, Fast, W. 2007 'Inhibition of human dimethylarginine dimethylaminohydrolase-1 by S-nitroso-L-homocysteine and hydrogen peroxide. Analysis, quantification, and implications for hyperhomocysteinemia.' *J Biol Chem.* vol. 282, no. 48, pp. 34684-92.

Hulin, J-A, Gubareva, EA, Jarzebska, N, Rodionov, RN, Mangoni, AA & Tommasi, S 2020, 'Inhibition of Dimethylarginine Dimethylaminohydrolase (DDAH) Enzymes as an Emerging Therapeutic Strategy to Target Angiogenesis and Vasculogenic Mimicry in Cancer', *Frontiers in Oncology*, vol. 9, no. 1455.

Hulin, J-A, Tommasi, S, Elliot, D, Hu, DG, Lewis, BC & Mangoni, AA 2017, 'MiR-193b regulates breast cancer cell migration and vasculogenic mimicry by targeting dimethylarginine dimethylaminohydrolase 1', *Scientific reports*, vol. 7, no. 1, p. 13996.

Hulin, J-A, Tommasi, S, Elliot, D & Mangoni, AA 2019, 'Small molecule inhibition of DDAH1 significantly attenuates triple negative breast cancer cell vasculogenic mimicry in vitro', *Biomedicine & Pharmacotherapy*, vol. 111, pp. 602-12.

Humm, A, Fritsche, E, Steinbacher, S & Huber, R 1997, 'Crystal structure and mechanism of human L-arginine:glycine amidinotransferase: a mitochondrial enzyme involved in creatine biosynthesis', *The EMBO journal*, vol. 16, no. 12, pp. 3373-85.

Isobe, C, Abe, T & Terayama, Y 2010, 'Decrease in Asymmetrical Dimethylarginine, an Endogenous Nitric Oxide Synthase Inhibitor, in Cerebrospinal Fluid during Elderly Aging and in Patients with Sporadic Form of Amyotrophic Lateral Sclerosis', *Neurosignals*, vol. 18, no. 1, pp. 43-8.

Kakimoto, Y & Akazawa, S 1970, 'Isolation and identification of N-G,N-G- and N-G,N'-G-dimethyl-arginine, N-epsilon-mono-, di-, and trimethyllysine, and glucosylgalactosyl- and galactosyl-delta-hydroxylysine from human urine', *The Journal of biological chemistry*, vol. 245, no. 21, pp. 5751-8.

Kami Reddy, KR, Dasari, C, Vandavasi, S, Natani, S, Supriya, B, Jadav, SS, Sai Ram, N, Kumar, JM & Ummanni, R 2019, 'Novel Cellularly Active Inhibitor Regresses DDAH1 Induced Prostate Tumor Growth by Restraining Tumor Angiogenesis through Targeting DDAH1/ADMA/NOS Pathway', *ACS Combinatorial Science*, vol. 21, no. 4, pp. 241-56.

Kawahara T. 1994 '[Experimental studies on effect on nitric oxide on the internal urethral relaxation in anesthetized rats]'. *Nihon Hinyokika Gakkai Zasshi*. vol. 85, no. 7, pp. 1124-30. Japanese.

Kotthaus, J, Schade, D, Kotthaus, J, Clement, B. 2012 'Designing modulators of dimethylarginine dimethylaminohydrolase (DDAH): a focus on selectivity over arginase.' *J Enzyme Inhib Med Chem.* vol. 27, no. 1, pp. 24-8.

Kittel, A & Maas, R 2014, 'Pharmacology and clinical pharmacology of methylarginines used as inhibitors of nitric oxide synthases', *Current pharmaceutical design*, vol. 20, no. 22, pp. 3530-47.

Knott, AB & Bossy-Wetzel, E 2009, 'Nitric oxide in health and disease of the nervous system', *Antioxidants & redox signaling*, vol. 11, no. 3, pp. 541-54.

Koss MC. 1999 'Functional role of nitric oxide in regulation of ocular blood flow.' *Eur J Pharmacol.* vol. 374, no. 2, pp. 161-74.

Kotthaus, J, Schade, D, Muschick, N, Beitz, E & Clement, B 2008, 'Structure–activity relationship of novel and known inhibitors of human dimethylarginine dimethylaminohydrolase-1: Alkenyl-amidines as new leads', *Bioorganic & Medicinal Chemistry*, vol. 16, no. 24, pp. 10205-9.

Kozlova, AA, Ragavan, VN, Jarzebska, N, Lukianova, IV, Bikmurzina, AE, Rubets, E, Suzuki-Yamamoto, T, Kimoto, M, Mangoni, AA, Gainetdinov, RR, Weiss, N, Bauer, M, Markov, AG,

Rodionov, RN & Bernhardt, N 2021, 'Divergent Dimethylarginine Dimethylaminohydrolase Isoenzyme Expression in the Central Nervous System', *Cell Mol Neurobiol*.

Lambden, S 2019, 'Bench to bedside review: therapeutic modulation of nitric oxide in sepsis—an update', *Intensive Care Medicine Experimental*, vol. 7, no. 1, p. 64.

Lawson, TN, Weber, RJM, Jones, MR, Chetwynd, AJ, Rodríguez-Blanco, G, Di Guida, R, Viant, MR & Dunn, WB 2017, 'msPurity: Automated Evaluation of Precursor Ion Purity for Mass Spectrometry-Based Fragmentation in Metabolomics', *Analytical Chemistry*, vol. 89, no. 4, pp. 2432-9.

Leiper, J & Nandi, M 2011, 'The therapeutic potential of targeting endogenous inhibitors of nitric oxide synthesis', *Nature Reviews. Drug Discovery*, vol. 10, no. 4, pp. 277-91.

Leiper, JM, Santa Maria, J, Chubb, A, MacAllister, RJ, Charles, IG, Whitley, GS & Vallance, P 1999, 'Identification of two human dimethylarginine dimethylaminohydrolases with distinct tissue distributions and homology with microbial arginine deiminases', *Biochem J*, vol. 343 Pt 1, no. 1, pp. 209-14.

Leitão, RFC, Ribeiro, RA, Bellaguarda, EAL, Macedo, FDB, Silva, LR, Oriá, RB, Vale, ML, Cunha, FQ & Brito, GAC 2007, 'Role of nitric oxide on pathogenesis of 5-fluorouracil induced experimental oral mucositis in hamster', *Cancer Chemother Pharmacol*, vol. 59, no. 5, pp. 603-12.

Levine, AB, Punihaole, D & Levine, TB 2012, 'Characterization of the Role of Nitric Oxide and Its Clinical Applications', *Cardiology*, vol. 122, no. 1, pp. 55-68.

Linsky, T, Wang, Y, Fast, W. 2011 'Screening for dimethylarginine dimethylaminohydrolase inhibitors reveals ebselen as a bioavailable inactivator.' *ACS Med Chem Lett*.; vol. 2, no. 8, pp. 592-596.

Liu, H, Weng, L & Yang, C 2017, 'A review on nanomaterial-based electrochemical sensors for H2O2, H2S and NO inside cells or released by cells', *Microchimica Acta*, vol. 184, no. 5, pp. 1267-83.

Liu, X, Xu, X, Shang, R & Chen, Y 2018, 'Asymmetric dimethylarginine (ADMA) as an important risk factor for the increased cardiovascular diseases and heart failure in chronic kidney disease', *Nitric Oxide*, vol. 78, pp. 113-20.

Lowry, O, Rosebrough, N, Farr, AL & Randall, R 1951, 'PROTEIN MEASUREMENT WITH THE FOLIN PHENOL REAGENT', *Journal of Biological Chemistry*, vol. 193, no. 1, pp. 265-75.

Luanpitpong, S & Chanvorachote, P 2015, 'Nitric Oxide and Aggressive Behavior of Lung Cancer Cells', *Anticancer Research*, vol. 35, no. 9, p. 4585.

Luiking, YC, Engelen, MPKJ & Deutz, NEP 2010, 'Regulation of nitric oxide production in health and disease', *Current opinion in clinical nutrition and metabolic care*, vol. 13, no. 1, pp. 97-104.

Lundgren, BR, Bailey, FJ, Moley, G & Nomura, CT 2017, 'DdaR (PA1196) Regulates Expression of Dimethylarginine Dimethylaminohydrolase for the Metabolism of Methylarginines in Pseudomonas aeruginosa PAO1', *Journal of bacteriology*, vol. 199, no. 8, pp. e00001-17.

Mangoni, AA, Ceruti, T, Frapolli, R, Russo, M, Fichera, S, Zucchetti, M & Tommasi, S 2022, 'Pharmacokinetic Characterization of the DDAH1 Inhibitors ZST316 and ZST152 in Mice Using a HPLC-MS/MS Method', *Molecules (Basel, Switzerland)*, vol. 27, no. 3, p. 1017.

Matsunaga, T, Weihrauch, DW, Moniz, MC, et al. 2002 'Angiostatin inhibits coronary angiogenesis during impaired production of nitric oxide.' *Circulation*. vol. 105, pp. 2185–2191.

Mishra, A & Newman, E 2012, 'Aminoguanidine Reverses the Loss of Functional Hyperemia in a Rat Model of Diabetic Retinopathy', *Frontiers in Neuroenergetics*, vol. 3.

Murphy, R, Tommasi, S, Lewis, B & Mangoni, A 2016, 'Inhibitors of the Hydrolytic Enzyme Dimethylarginine Dimethylaminohydrolase (DDAH): Discovery, Synthesis and Development', *Molecules*, vol. 21, p. 615.

Murray-Rust, J, Leiper, J, McAlister, M, Phelan, J, Tilley, S, Maria, JS, Vallance, P & McDonald, N 2001, 'Structural insights into the hydrolysis of cellular nitric oxide synthase inhibitors by dimethylarginine dimethylaminohydrolase', *Nature structural biology*, vol. 8, no. 9, pp. 818-.

Nandi, M, Kelly, P, Torondel, B, Wang, Z, Starr, A, Ma, Y, Cunningham, P, Stidwill, R & Leiper, J 2012, 'Genetic and pharmacological inhibition of dimethylarginine dimethylaminohydrolase 1 is protective in endotoxic shock', *Arterioscler Thromb Vasc Biol*, vol. 32, no. 11, pp. 2589-97.

Ogawa, T, Kimoto, M & Sasaoka, K 1987, 'Occurrence of a new enzyme catalyzing the direct conversion of NG,NG-dimethyl-L-arginine to L-citrulline in rats', *Biochemical and Biophysical Research Communications*, vol. 148, no. 2, pp. 671-7.

Ogawa, T, Kimoto, M & Sasaoka, K 1990, 'Dimethylarginine:pyruvate aminotransferase in rats. Purification, properties, and identity with alanine:glyoxylate aminotransferase 2', *The Journal of biological chemistry*, vol. 265, no. 34, pp. 20938-45.

Opatrilova, R, Kubatka, P, Caprnda, M, Büsselberg, D, Krasnik, V, Vesely, P, Saxena, S, Ruia, S, Mozos, I, Rodrigo, L, Kruzliak, P & dos Santos, KG 2018, 'Nitric oxide in the pathophysiology of retinopathy: evidences from preclinical and clinical researches', *Acta Ophthalmologica*, vol. 96, no. 3, pp. 222-31.

Ota, M, Crofton, JT, Festavan, GT, Share, L, 1993 'Evidence that Nitric Oxide Can Act Centrally to Stimulate Vasopressin Release', *Neuroendocrinology*, vol. 57, no. 5, pp. 955-959.

Palm, F, Onozato, ML, Luo, Z & Wilcox, CS 2007, 'Dimethylarginine dimethylaminohydrolase (DDAH): expression, regulation, and function in the cardiovascular and renal systems', *American Journal of Physiology-Heart and Circulatory Physiology*, vol. 293, no. 6, pp. H3227-H45.

Paul, D, Sanap, G, Shenoy, S, Kalyane, D, Kalia, K & Tekade, RK 2021, 'Artificial intelligence in drug discovery and development', *Drug Discovery Today*, vol. 26, no. 1, pp. 80-93.

Picón-Pagès, P, Garcia-Buendia, J & Muñoz, FJ 2019, 'Functions and dysfunctions of nitric oxide in brain', *Biochimica et Biophysica Acta (BBA) - Molecular Basis of Disease*, vol. 1865, no. 8, pp. 1949-67.

Pullamsetti, SS, Savai, R, Dumitrascu, R, Dahal, BK, Wilhelm, J, Konigshoff, M, Zakrzewicz, D, Ghofrani, HA, Weissmann, N, Eickelberg, O, Guenther, A, Leiper, J, Seeger, W, Grimminger, F & Schermuly, RT 2011, 'The Role of Dimethylarginine Dimethylaminohydrolase in Idiopathic Pulmonary Fibrosis', *Science Translational Medicine*, vol. 03, no. 87, pp. 87ra53-87ra53.

Rees DD, Palmer RM, Hodson HF, Moncada S. 1989 'A specific inhibitor of nitric oxide formation from L-arginine attenuates endothelium-dependent relaxation.' *Br J Pharmacol.* vol. 96, no. 2, pp. 418-424.

Rossig L, Fichtlscherer B, Breitschopf K, et al. 1999 'Nitric oxide inhibits caspase-3 by S-nitrosation in vivo.' *J Biol Chem.* vol. 274, pp. 6823–6826.

Röszer, T 2012, 'The Biology of Subcellular Nitric Oxide', in pp. 179-85.

Santa Maria, J, Vallance, P, Charles, IG & Leiper, JM 1999, 'MicroCorrespondence: Identification of microbial dimethylarginine dimethylaminohydrolase enzymes', *Molecular Microbiology*, vol. 33, no. 6, pp. 1278-9.

Seymour, M, Pétavy, F, Chiesa, F, Perry, H, Lukey, PT, Binks, M, Donatien, PD, Freidin, AJ, Eckersley, RJ & McClinton, C 2012, 'Ultrasonographic measures of synovitis in an early phase clinical trial: a double-blind, randomised, placebo and comparator controlled phase IIa clinical trial of GW274150 (a selective inducible nitric oxide synthase inhibitor) in rheumatoid arthritis', *Clinical and Experimental Rheumatology-Incl Supplements*, vol. 30, no. 2, p. 254.

Shen, C-H 2019, 'Chapter 8 - Quantification and Analysis of Proteins', in C-H Shen (ed.), *Diagnostic Molecular Biology*, Academic Press, pp. 187-214.

Singh, S & Dikshit, M 2007, 'Apoptotic neuronal death in Parkinson's disease: Involvement of nitric oxide', *Brain Research Reviews*, vol. 54, no. 2, pp. 233-50.

Soliman, MM 2014, 'Effects of aminoguanidine, a potent nitric oxide synthase inhibitor, on myocardial and organ structure in a rat model of hemorrhagic shock', *Journal of emergencies, trauma, and shock*, vol. 7, no. 3, pp. 190-5.

Stamler JS, Loh E, Roddy MA, Currie KE, Creager MA. 1994 'Nitric oxide regulates basal systemic and pulmonary vascular resistance in healthy humans.' *Circulation*, vol. 89, no. 5, pp. 2035-40.

Stone, EM, Schaller, TH, Bianchi, H, Person, MD & Fast, W 2005, 'Inactivation of two diverse enzymes in the amidinotransferase superfamily by 2-chloroacetamidine: dimethylargininase and peptidylarginine deiminase', *Biochemistry*, vol. 44, no. 42, pp. 13744-52.

Stuehr DJ, Marletta MA. 1985 'Mammalian nitrate biosynthesis: mouse macrophages produce nitrite and nitrate in response to *Escherichia coli* lipopolysaccharide.' *Proc Natl Acad Sci U S A*., vol. 82, no. 22, pp. 7738-7742.

Swiech, K, Picanço-Castro, V & Covas, DT 2012, 'Human cells: New platform for recombinant therapeutic protein production', *Protein Expression and Purification*, vol. 84, no. 1, pp. 147-53.

Tain,, YL & Hsu, CN 2017, 'Toxic Dimethylarginines: Asymmetric Dimethylarginine (ADMA) and Symmetric Dimethyla rginine (SDMA)', *Toxins*, vol. 9, no. 3, p. 92.

Thomas, P & Smart, TG 2005, 'HEK293 cell line: a vehicle for the expression of recombinant proteins', *J Pharmacol Toxicol Methods*, vol. 51, no. 3, pp. 187-200.

Toda N, Okamura, T 2011 'Modulation of renal blood flow and vascular tone by neuronal nitric oxide synthase-derived nitric oxide.' *J Vasc Res.*, vol. 48, no. 1, pp. 1-10.

Tojo, A, Kimoto, M & Wilcox, CS 2000, 'Renal expression of constitutive NOS and DDAH: Separate effects of salt intake and angiotensin', *Kidney international*, vol. 58, no. 5, pp. 2075-83.

Tojo, A, Welch, WJ, Bremer, V, Kimoto, M, Kimura, K, Omata, M, Ogawa, T, Vallance, P & Wilcox, CS 1997, 'Colocalization of demethylating enzymes and NOS and functional effects of methylarginines in rat kidney', *Kidney Int*, vol. 52, no. 6, pp. 1593-601.

Tommasi, S, Elliot, DJ, Hulin, JA, Lewis, BC, McEvoy, M & Mangoni, AA 2017, 'Human dimethylarginine dimethylaminohydrolase 1 inhibition by proton pump inhibitors and the cardiovascular risk marker asymmetric dimethylarginine: in vitro and in vivo significance', *Scientific Reports (Nature Publisher Group)*, vol. 7, pp. 1-10.

Tommasi, S, Zanato, C, Lewis, BC, Nair, PC, Dall'Angelo, S, Zanda, M & Mangoni, AA 2015, 'Arginine analogues incorporating carboxylate bioisosteric functions are micromolar inhibitors of human recombinant DDAH-1', *Organic & Biomolecular Chemistry*, vol. 13, no. 46, pp. 11315-30.

Tran, CTL, Fox, MF, Vallance, P & Leiper, JM 2000, 'Chromosomal Localization, Gene Structure, and Expression Pattern of DDAH1: Comparison with DDAH2 and Implications for Evolutionary Origins', *Genomics*, vol. 68, no. 1, pp. 101-5.

Unlu, A, Onmaz, DE, Abusoglu, S & Abusoglu, G 2021, 'HPLC and LC-MS/MS measurement methods for the quantification of asymmetric dimethylarginine (ADMA) and related metabolites', *Turkish Journal of Biochemistry*, vol. 46, no. 4, pp. 327-47.

Vallance, P & Leiper, J 2004, 'Cardiovascular Biology of the Asymmetric Dimethylarginine:Dimethylarginine Dimethylaminohydrolase Pathway', *Arterioscler Thromb Vasc Biol*, vol. 24, no. 6, pp. 1023-30.

Vallance, P, Leone, A, Calver, A, Collier, J & Moncada, S 1992, 'Accumulation of an endogenous inhibitor of nitric oxide synthesis in chronic renal failure', *Lancet (London, England)*, vol. 339, no. 8793, pp. 572-5.

Wang, Y, Hu, S, Gabisi Jr, AM, Er, JAV, Pope, A, Burstein, G, Schardon, CL, Cardounel, AJ, Ekmekcioglu, S & Fast, W 2014, 'Developing an Irreversible Inhibitor of Human DDAH-1, an Enzyme Upregulated in Melanoma', *ChemMedChem*, vol. 9, no. 4, pp. 792-7.

Wang Z, Lambden S, Taylor V, Sujkovic E, Nandi M, Tomlinson J, Dyson A, McDonald N, Caddick S, Singer M, Leiper J 2014 'Pharmacological inhibition of DDAH1 improves survival, haemodynamics and organ function in experimental septic shock.' *Biochem J*. vol. 460, no. 2, pp. 309-16.

Weist, S, Eravci, M, Broedel, O, Fuxius, S, Eravci, S & Baumgartner, A 2008, 'Results and reliability of protein quantification for two-dimensional gel electrophoresis strongly depend on the type of protein sample and the method employed', *PROTEOMICS*, vol. 8, no. 16, pp. 3389-96.

Wilcken, DEL, Sim, AS, Wang, J & Wang, XL 2007, 'Asymmetric dimethylarginine (ADMA) in vascular, renal and hepatic disease and the regulatory role of l-arginine on its metabolism', *Mol Genet Metab*, vol. 91, no. 4, pp. 309-17.

Wolff, DJ & Lubeskie, A 1995, 'Aminoguanidine Is an Isoform-Selective, Mechanism-Based Inactivator of Nitric Oxide Synthase', *Archives of Biochemistry and Biophysics*, vol. 316, no. 1, pp. 290-301.

Wu, CC, Chen, SJ, Szabó, C, Thiemermann, C & Vane, JR 1995, 'Aminoguanidine attenuates the delayed circulatory failure and improves survival in rodent models of endotoxic shock', *Br J Pharmacol*, vol. 114, no. 8, pp. 1666-72.

Yki-Järvinen, H, Bergholm, R & Leirisalo-Repo, M 2003, 'Increased inflammatory activity parallels increased basal nitric oxide production and blunted response to nitric oxide in vivo in rheumatoid arthritis', *Ann Rheum Dis*, vol. 62, no. 7, pp. 630-4.

Zhang, HQ, Fast, W, Marletta, MA, Martasek, P & Silverman, RB 1997, 'Potent and Selective Inhibition of Neuronal Nitric Oxide Synthase by Nω-Propyl-l-arginine', *Journal of Medicinal Chemistry*, vol. 40, no. 24, pp. 3869-70.

Zhao, W, Tilton, RG, Corbett, JA, McDaniel, ML, Misko, TP, Williamson, JR, Cross, AH & Hickey, WF 1996, 'Experimental allergic encephalomyelitis in the rat is inhibited by aminoguanidine, an inhibitor of nitric oxide synthase', *Journal of neuroimmunology*, vol. 64, no. 2, pp. 123-33.

Zhu, L, Wang, X, Song, X, Zheng, F, Li, H, Chen, F, Zhang, Y & Zhang, F 2020, 'Evolution of the key odorants and aroma profiles in traditional Laowuzeng baijiu during its one-year ageing', *Food Chemistry*, vol. 310, p. 125898.

APPENDICCES

APPENDIX A - Solution preparation

Acrylamide gel (10%) – Separating gel
15 mL
5.6 mL of 1 M Tris, pH 8.8, 3.75 mL of acrylamide/ Bis 40%, 75 µL of 20% SDS, 75 µL of 10% APS, 7.5 µL of Temed were added to 5.55 mL of of MilliQ water.

Acrylamide gel (4%) – Stacking gel
10 mL
1.25 mL of 1 M Tris, pH 6.8, 1 mL of acrylamide/ Bis 40%, 50 µL of 20% SDS, 50 µL of 10% APS, 10 µL of Temed were added to 7.4 mL of of MilliQ water.

10% APS
10 mL stock
1 g of APS dissolved in 10 mL of of MilliQ water. Aliquoted in to 200 µL.

4% BLOTTO
2 g of skim milk powder were dissolved in 40 mL of TBST.

BSA
1 mL stock (10 mg/mL)
100 µL of BSA added to 900 µL of MilliQ water.

CIT
1 mL stock at 80 µM
8 µL of CIT added to 992 µL of MilliQ water.

CIT-d6
500 µL at 50 µM
250 µL of CIT-d6 at 100 µM added to 250 µL of MilliQ water.

Comassie Blue de-stain
550 mL stock
225 mL of 45% (v/v) methanol, 50 mL of 10% acetic acid were added to 225 mL of MilliQ water.

Comassie Blue Staining
250 mL stock
125 mL of 50% methanol, 25 mL of 10% (v/v) acetic acid, 250 g of 0.1% Comassie Blue Staining solution G-250 were added to 100 mL of MilliQ water.

DMEM complete medium
2 L stock
26.96 g of DMEM powder, 7.4 g of sodium bicarbonate, 20 mL of MEM, 20 mL of sodium pyruvate 100 mM were dissolved into 1.5 mL of MilliQ water. The pH was adjusted to 7.4 by

using concentrated hydrochloric acid and the solution, then complete with MilliQ water until reaches 2 L. Media was filtered using sterilised filter (0.2 µm) in a tissue culture hood. 1 mL of antibiotic puromycin (1 mg/mL) and 10%FBS were added to complete the medium.
Incomplete medium
The incomplete medium was aliquoted in 900 mL fractions into 1 L sterile bottles and stored at 4-8 °C. Prior to use, 100 mL of Foetal Bovine Serum (10% FBS) and 1 mL puromycin (final concentration 1 µg/mL) of were added to the 900 mL DMEM aliquot for a total volume of 1 L of complete DMEM.

EZQ destain
500 mL stock
50 mL of 10% methanol, 35 mL of 7% acetic acid were added into 415 mL of MilliQ water.

Ovalbumin
2.0 mg/mL stock
200 µL of ovalbumin at 10 mg/mL added to 800 µL of MilliQ water.

1 x Phosphate Buffered Saline (PBS)
1 L stock
8 g of NaCl, 200 mg of KCl, 1.44 g of Na_2HPO_4, 245 mg of KH_2PO_4 were dissolved into 800 mL of MilliQ water (Merck, Australia). The pH was adjusted to 7.4 using NaOH.

1 M Potassium phosphate buffer
100 mL stock
For pH 7.4 phosphate buffer 80.2 mL of 1 M K_2HPO_4 were added to 19.8 mL of 1 M KH_2PO_4. For 100 mL 1 M K_2HPO_4 17.418 g K_2HPO_4 were dissolved into 100 mL of MilliQ water. For 100 mL 1 M KH_2PO_4 13.609 g KH_2PO_4 were dissolved into 100 mL of MilliQ water.

10x Running Buffer
2.5 L stock
75.75 g of 25 mM Trizma base, 360 g of 192 mM glycine, 25 g of SDS 0.1% were dissolved into 2.5 L of MilliQ water.

1x Running Buffer
500 mL stock
50 mL of 10x running buffer added to 450 mL of MilliQ water.

SDS Sample buffer Dye
10 mL stock
2.5 mL of 1 M Tris-base pH 6.8,4 mL of 50% v/v glycerol, 0.8 g of 5% w/v SDS, 0.8 mL of 250 mM dithiothreoitol and 40 mg of 0.2% w/v bromophenol blue were added to 10 mL of MilliQ water.

20% SDS
100 mL stock
20 g SDS dissolved in 100 mL of MilliQ water.

TBST
1 L stock
2 mL of Tween 20 were added to 1 L of 1 x TBS.

1 M Tris pH 8.8
500 mL stock
60.55 g of Tris dissolved in 450 mL of MilliQ water. The pH was adjusted to 8.8 using NaOH.

1 M Tris pH 6.8
100 mL stock
12.11 g of Tris dissolved in 90 mL of MilliQ water. The pH was adjusted to 6.8 using HCl

10x Transfer Buffer
2.5 L stock
75.75 g of 25 mM Trizma base, 360 g of 192 mM glycine were dissolved into 2.5 L of MilliQ water.

1x Transfer Buffer
1 L stock
200 mL of cold methanol 20%, 100 mL cold 10 x transfer buffer added to 100 mL of MilliQ water.

10x Tris buffered saline (TBS)
2.5 L stock
151.5 g of 0.5 M Tris, 219 g of 1.5 M sodium chloride (NaCl) were dissolved into 2.5 L of MilliQ water. The pH was adjusted to 7.4 using aqueous HCL or NaOH as required.

1x TBS
1 L stock
100 mL of 10x TBS added to 900 mL of MilliQ water.

APPENDIX B – Equipment, Consumables and Software

Table 8: List of used Equipment, Consumables and Software

CONSUMABLES	SUPPLIER
0.2 µm filter vacucap	Merck, NSW, Australia
0.45 µm trans-blot nitrocellulose membrane	Bio-Rad Laboratories, CA, USA
Multi-channel Pipettor	Eppendorf South Pacific, NSW, Australia
Nitrocellulose	Bio-Rad Laboratories, CA, USA
Pasteur pipette	Adelab Scientific, SA, Australia
Pipette single channel (P10, P100, P200, P1000, P5000)	Eppendorf South Pacific, NSW, Australia
Pipette (P5, P20, P200, P1000)	Gilson through John Morris Scientific, NSW, Australia
Tissue culture flask (T75/ T175)	ThermoFisher Scientific, VIC, Australia
Tubes – safe lock	Eppendorf South Pacific, NSW, Australia
Whatman paper	Merck, NSW, Australia
EQUIPMENT	**SUPPLIER**
Bio-safety Cabinet	Labconco, MO, USA
ChemiDoc Touch Imaging System	Bio-Rad Laboratories, CA, USA
CKX53 Cell Culture Microscope	Olympus, Tokyo, Japan
Incubator cell culture	SANYO, Osaka, Japan
Laminar Floor Hoods	AES Environment/ Gelman Sciences, NSW, Australia
Shaker	ThermoFisher Scientific, VIC, Australia
Sonicator	Sonics, CT, USA
SpectraMax iD5 plate reader	FMC – Proteomic facility, SA, Asutralia
Waters Atlantis HILIC column (3 µm, 2.1 mm x 150 mm)	Waters Australia, NSW, Australia
Wester Blotting apparatus	Bio-Rad Laboratories, CA, USA
Waters ACQUITY™ Ultra Performance LC™	Waters Australia, NSW, Australia
Waters Premier quadrapole time of flight (qToF) mass spectrometer	Waters Australia, NSW, Australia
SOFTWARE	**MANUFACTURER**
Microsoft Excel	Microsoft Office 365 ProPlus, Microsoft Corporation, NM, USA
Prism	GraphPad, CA, USA
ImageLab	Bio-Rad Laboratories, CA, USA
MassLynx version 4.1	Waters Australia, NSW, Australia